5-13-2017

Measurement of the Longitudinal Double-spin Asymmetry for Neutral Pion Production in Polarized Proton Collisions at $\sqrt{s}$ = 510 GeV

Taegyun Kim
Valparaiso University

Follow this and additional works at: http://scholar.valpo.edu/phys_astro_honors

Part of the Physics Commons

Measurement of the Longitudinal Double-spin Asymmetry for Neutral Pion Production in Polarized Proton Collisions at $\sqrt{s} = 510 \; GeV$

Taegyun Kim

Mentor : Dr. Adam Gibson-Even

May 13, 2017

Contents

Chapter 1

Introduction

1.1 Abstract

Beyond the valence quarks' spin contribution to the total spin of a proton, gluon and sea quark contributions are becoming clear as well. For proton+proton collisions at a center of mass energy of 510 GeV, neutral pion production is dominated by gluon-gluon and gluon-quark scattering. An avenue to constrain the gluon polarization is the asymmetry, A_{LL}, in the production of neutral pions from collisions of longitudinally spin-polarized proton beams. Our experiment was performed with the STAR detector at the Relativistic Heavy Ion Collider (RHIC), unique for its ability to collide spin-polarized proton beams. The Endcap Electromagnetic Calorimeter (EEMC) of the STAR detector with its pseudo-rapidity (η) range between 1.09 and 2.00 and full azimuthal coverage measures energies of photons from π^0 decays. We consider the invariant mass of all photon pairs in the EEMC as we identify π^0 candidates. We will present the current status of the analysis of the π^0 A_{LL} as measured by the EEMC at STAR in 2012 data with center-of-mass energy of 510 GeV.
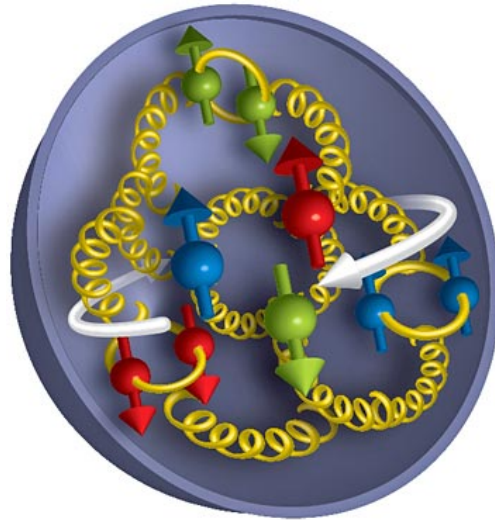
1.2   Overview

Figure 1.1: Structure of a proton [1]

In the Standard Model of particle physics, we know the individual constituents of the proton, such as quarks with spin $\frac{1}{2}$ and gluons with spin 1 in standard units. In a simple proton model, two up quarks and one down quark consists a proton, which are sufficient to explain the charge contribution of each constituent. However, as shown in Figure 1.1, the partonic structure of the proton is more complicated, in a sense that the specific spin contributions of gluons are hard to determine. In other words, total spin of a proton is not solely governed by quarks. In addition to the complicity in structure, each constituent has the orbital motion relative to others. All of the contribution factors add up to a proton's spin of $\frac{1}{2}$. This experimental analysis seeks to enhance our understanding of the role of the proton's constituents, specifically the gluons, in making up the spin of the proton. Due to the incompetence of performing direct measurements of spin contributions for each constituent type, we can analyze the phenomenons of products after colliding two protons in order to understand the properties of individual parts that consists a proton. The Relativistic Heavy Ion Collider (RHIC) at Brookhaven National Lab (BNL) has performed spin polarized collisions of proton+proton in order to probe the inner structure of proton. The Solenoidal Tracker At RHIC (STAR) is one of two detectors that are being used for investigating gluons' spin contribution. SThe STAR detector is distinctive in that it has full azimuthal coverage, which will be further discussed in later section.
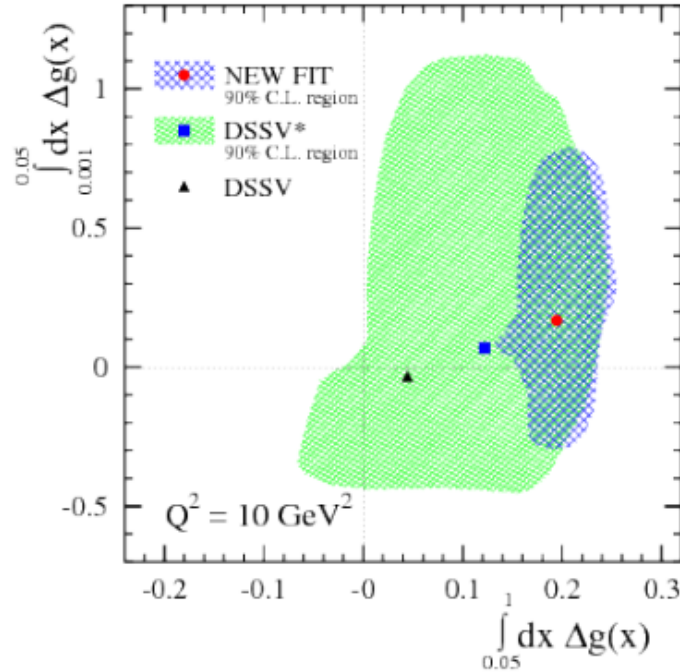
1.3   Physical Motivation

Figure 1.2: DSSV analysis based on RHIC data [1]
The C.L (Confidence Level) area spanned by each momentum fraction carried by a parton, x_{bj}, shows the uncertainty range. Δg is the partonic gluon spin contribution aligned with the proton's spin. New DSSV fit shows significantly reduced uncertainty range at $0.05 < x_{bj} < 1$, yet $0.001 < x_{bj} < 0.05$ still has high uncertainty region. DSSV is a detailed account of the first global analysis of polarized Parton Distribution Functions presented [2].

RHIC's spin polarized $p + p$ collision data have been analyzed previously with 2006 data with center of mass energy with 200 GeV by STAR collaboration [3] and PHENIX collaboration [4]. These research papers provide the constrained gluons' spin contributions about 25 percent of a proton's total intrinsic spin for $x_{bj} > 0.002$ (Figure 1.2). Valparaiso University have been involved in 2006 data analysis [3], and provided results at specific π^0 transverse momentum (p_T) range, $5 < p_T < 12\,GeV/c$. In 2012, STAR collected a very large dataset at higher $p + p$ collision energy with developments in the detector, and the 2012 dataset contains about 10 times the number of collision events. Historically, the DSSV fit, figure 1.2, has been improved: blue data point (DSSV*) with green uncertainty region had been shrunk down to new fit with less uncertainty. For x-axis when momentum fraction carried by gluons is between 0.05 and 1, it is clear non$-$zero spin contribution of gluons. Unlike to this, lower momentum fraction carried by gluons ($0.001 < \Delta g < 0.05$) is yet not sufficiently evaluated to investigate the clearer spin contribution. From 2012 dataset with higher collision energy, we expect to obtain results at lower momentum gluons ($x_{bj} < 0.05$, y-axis of the figure). Our data analysis is done for pseudo-rapidity (η) between 1.1 to 2.0 (intermediate pseudo-

rapidity region) by the Endcap ElectroMagnetic Calorimeter (EEMC). This result can be used to cross check with the analysis results from data collected by Barrel ElectroMagnetic Calorimeter (BEMC) or Forward Meson Spectrometer (FMS). Our major goal is to extend the 2006 analysis to the 2012 dataset and we hope that theorists will be able to produce fits with reduced uncertainty at low x_{bj}.

1.4   Theoretical Background

1.4.1   Proton Spin Structure

The proton's spin in a realistic model of the proton can be written as the sum of four spin contributers written as:

$$S_{p^+} = \frac{1}{2}\Delta\Sigma + \Delta G + L_q + L_G = \frac{1}{2} \tag{1.1}$$

In Equation 1.1, S_{p^+} denotes the total intrinsic spin of the proton. $\Delta\Sigma$ denotes the polarization of quarks - both valence quarks and sea quarks[1]. This quarks' spin term carries coefficient of $\frac{1}{2}$ since quarks are fermions. ΔG denotes the gluons' spin contribution; and $L_{q,G}$ denotes the orbital angular momentum for each respective parton.

For this research, we will concentrate on constraining the ΔG, called gluons' polarization inside a proton. For a spin-polarized proton, parton's polarization can be written as:

$$\Delta f(x, Q^2) = f^+(x, Q^2) - f^-(x, Q^2) \tag{1.2}$$

$$f(x, Q^2) = f^+(x, Q^2) + f^-(x, Q^2) \tag{1.3}$$

Equation 1.2 means preference of a parton at a given state, $f(x, Q^2)$, relative to the spin of a proton which is expressed as the difference between f^+ (polarization of partons along the polarization of a proton) and f^- (opposite partonic polarization relative to the proton's polarization) whereas the spin of unpolarized parton, equation 1.3, is expressed as sum of f^+ and f^-. x represents the fraction of the proton's momentum carried by specific parton (also known as Bjorken Parameter, x_{bj}). Q^2 represents the momentum carried by the proton. For any partons in a proton, total polarization can be derived by integrating over x_{bj}. Applying this to the gluon, ΔG represents the preference of gluons' spin alignment relative to the proton's spin.

---

[1]Sea quarks are the virtual quarks that appear in first order of gluon's interaction Feynman Diagram between two quarks in general. The production of the sea quarks occurs in quark-antiquark pairs.

1.4.2   Kinematics of p+p Helicity Oriented Collisions

First, in phenomenological aspect, the one-to-one collision of two partons can be expressed using cross section of the collision and its relationship with the longitudinal double spin asymmetry (A_{LL}). The asymmetry is written as:

$$A_{LL} = \frac{d\sigma_{++} - d\sigma_{+-}}{d\sigma_{++} + d\sigma_{+-}} = \frac{\Delta d\sigma}{d\sigma} \tag{1.4}$$

This longitudinal double spin asymmetry includes the cross section (σ) differences depending on the colliding protons' spin structure. For our experiment, the spin differences are in longitudinal orientation (helicity). For polarized proton + proton collisions, we are interested in a specific process, $\vec{p}\vec{p} \rightarrow \pi^0 X$, which was used for theoretical A_{LL} calculation (the vector sign above the p denotes that the proton is longitudinally polarized). The differences were expressed using the QCD Factorization Theorem cross section analysis [5]:

$$\Delta d\sigma / d\Omega = \Delta d\sigma^{\vec{p}\vec{p} \rightarrow \pi^0 X} / d\Omega$$

$$= \int_{p_T^{min}} dp_T \sum_{ff' \rightarrow iX} \int dx_1 dx_2 dz \, \Delta f^p(x_1) \, \times \, \Delta f'^p(x_2) \, \times \, D_i^{\pi^0}(z) \, \times \, \frac{\Delta d\sigma^{\vec{f}\vec{f'} \rightarrow iX}}{d\Omega} \tag{1.5}$$

Equation 1.5 shows the theoretical expression for polarized cross section at unit solid angle for the proton pair ($d\Omega$). The equation is integrated over all transverse momentum (p_T) range, and summed over the partonic hard scattering processes ($ff' \rightarrow iX$). $f(x)$ indicates the Parton Distribution Function (PDF) of a proton, which represents the initial conditions of the collision and fragmentation function ($D_i^{\pi^0}$) represents the final condition of the collision. These initial and final conditions were mediated by the partonic cross section ($\Delta d\sigma^{\vec{f}\vec{f'} \rightarrow iX}$) of the specific process. For unpolarized cross section ($d\sigma$), Δ will be removed from the previous equation (1.5). The kinematic processes of the p+p collisions were dominated by scattering of quark+gluon (qg) and gluon+gluon (gg). Theoretical A_{LL} can be obtained by dividing unpolarized cross section from the polarized cross section.

$$A_{LL} = \frac{\int_{p_T^{min}} dp_T \sum_{ff' \rightarrow iX} \int dx_1 dx_2 dz \, \Delta f^p(x_1) \, \times \, \Delta f'^p(x_2) \, \times \, D_i^{\pi^0}(z) \, \times \, \Delta d\sigma^{\vec{f}\vec{f'} \rightarrow iX}}{\int_{p_T^{min}} dp_T \sum_{ff' \rightarrow iX} \int dx_1 dx_2 dz \, f^p(x_1) \, \times \, f'^p(x_2) \, \times \, D_i^{\pi^0}(z) \, \times \, d\sigma^{ff' \rightarrow iX}} \tag{1.6}$$

With simplification, this equation is rewritten as

$$A_{LL} \approx \frac{\Delta f_1(x_{bj}, Q^2)}{f_1(x_{bj}, Q^2)} \cdot \frac{\Delta f_2(x_{bj}, Q^2)}{f_2(x_{bj}, Q^2)} \alpha_{LL} \tag{1.7}$$

Equation 1.7 shows the final simplified version of theoretically calculated double spin asymmetry. α is called process-specific spin-correlation coefficient predicted by perturbative Quantum Chromo-Dynamics (pQCD), which is defined as $\alpha_{LL} = \Delta d\sigma^{ff' \to iX} / d\sigma^{ff' \to iX}$ (in other words, α_{LL} represents partonic asymmetry). Each $\frac{\Delta f}{f}$ represents the partonic spin contribution, in other words, the likelihood of parton's spin that is aligned with the proton's spin direction.
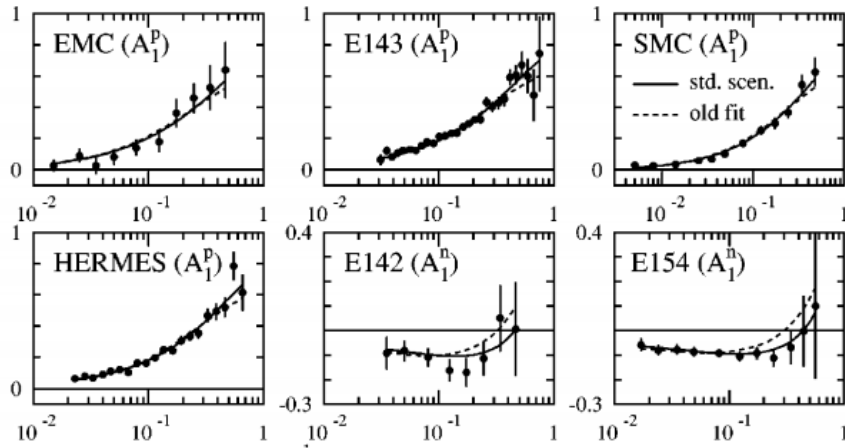

Figure 1.3: Proton quark spin asymmetry [6]

In Figure 1.3, A_1^p represents polarized partonic spin contribution based on analysis of polarized deep inelastic lepton-hadron scattering experiment, and this quantity can be substituted by $\frac{\Delta f}{f}$ from the previous A_{LL} equation. CERN and SLAC had been involved in this research in order to investigate A_1^p (proton), A_1^n (neutron). This A_1 represents the quark spin asymmetry, which clearly shows the spin contribution differences for a proton (p) and a neutron (n).

1.4.3 Longitudinal Double Spin Asymmetry (A_{LL})

Measuring of longitudinal double spin asymmetry (A_{LL}) comes from the cross section measurement of the collisions at specific helicity states. In this section, we will apply the theoretical calculation to the experimental aspect. A_{LL} can be written in terms of neutral pion production asymmetry that can be measured by the experiment:

$$A_{LL} = \frac{\sigma_{++} - \sigma_{+-}}{\sigma_{++} + \sigma_{+-}} = \frac{1}{P_Y \, P_B} \cdot \frac{\frac{N_{++}}{L_{++}} - \frac{N_{+-}}{L_{+-}} - \frac{N_{-+}}{L_{-+}} + \frac{N_{--}}{L_{--}}}{\frac{N_{++}}{L_{++}} + \frac{N_{+-}}{L_{+-}} + \frac{N_{-+}}{L_{-+}} + \frac{N_{--}}{L_{--}}} \tag{1.8}$$

In Equation 1.8, we can calculate the A_{LL} by spin-dependent neutral pion production. Note that the helicity (longitudinal spin-orientation) is written as: $++, -+, +-, --$ where $+$ denotes the helicity direction of the proton is parallel to its momentum and $-$ represents the proton's helicity is anti-parallel to its momentum direction. $N_{helicity}$[2] is the number of neutral pion (π^0) produced at specific proton helicity collisions and $L_{helicity}$[3] denotes the luminosity of the collision events. Luminosity means the number of collision events per unit area per unit time. Each P_Y and P_B denotes the polarization correction factor of incident proton beam (one beam as yellow(Y) and another beam as blue(B)). For our experiment, polarization factor was measured by polarimetry group, each polarization of the beam is recorded fill by fill with information of time dependency [4].

$$A_{LL} = \frac{1}{P_Y \, P_B} \cdot \frac{N_{++} + N_{--} - R_3 \left(N_{+-} + N_{-+} \right)}{N_{++} + N_{--} + R_3 \left(N_{+-} + N_{-+} \right)} \tag{1.9}$$

$$R_3 = \frac{L_{++} + L_{--}}{L_{+-} + L_{-+}} \tag{1.10}$$

For our analysis, we used Equation 1.9 with an assumption and approximations. Detailed derivation of Equation 1.9 and 1.10 is included in Appendix 7.1.

---

[2] $N_{++}, N_{-+}, N_{+-}, N_{--}$
[3] $L_{++}, L_{-+}, L_{+-}, L_{--}$
[4] The specific information can be found in https://wiki.bnl.gov/rhicspin/Run_12_polarization

1.4.4 π^0 Detection and Reconstruction

Inaccessibility in direct detection of π^0

Figure 1.4: π^0 constituents

Neutral pion (π^0) is a particle with a short lifetime of $(8.52 \pm 0.18) \times 10^{-17}\,s$ with estimated path length of $25.5\,nm$. This feature constrains the direct measurement of π^0. And the rest mass of π^0 equals to $134.9766 \pm 0.0006\,MeV/c^2$. Since 98 % of π^0 decays into two photons, we measure the photons' energies with their opening angle, in order to reconstruct into the π^0. The importance of π^0 mass comes from the physical property that the particle's mass is invariant in all frame of reference.
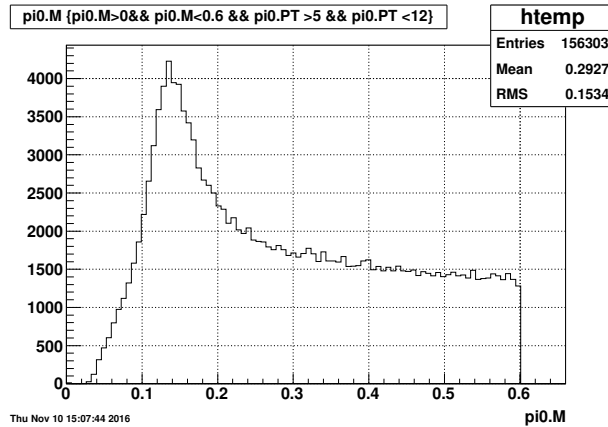

Figure 1.5: π^0 mass distribution

$$M_{\gamma\gamma} = (E_1 + E_2) \cdot \sqrt{\left(1 - \left(\frac{E_1 - E_2}{E_1 + E_2}\right)^2\right) \sin\frac{\theta}{2}} \tag{1.11}$$

Figure 1.5 is an example of a mass distribution plot. Invariant mass calculation was done in order to generate the distribution. Since we cannot specifically identify which photon came from which pion, we consider all combinations of two photons with their opening angle. Equation 1.11 was used for mass distribution calculation. Mass distributions like figure 1.5 include both "signal" and "background". "Signal" is the real π^0 that is produced due to the proton+proton collisions and "background" includes the wrong combinations that does not lie under the π^0 mass region. In this equation, each E is the energy of a photon and θ equals to the opening angle of two selected photons. From Figure 1.5, we can see the peak

at around $135\,MeV/c^2$ where π^0 invariant mass lies. Invariant mass is a characteristic of an object that is the same in all frames of reference. Therefore, even knowing the properties of produced photons from the decay, we can calculate invariant mass in order to determine whether it is located within the reasonable boundary of known π^0 mass.

Chapter 2

Experimental Method

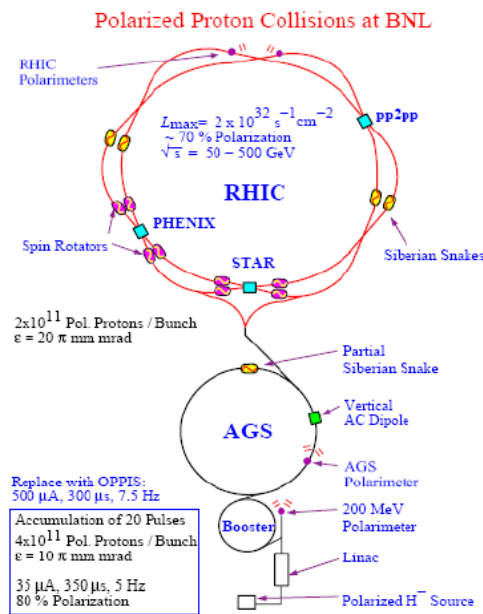## 2.1 Spin Polarized Collisions at RHIC

Figure 2.1: Relativistic Heavy Ion Collider (RHIC) schematic [7]

Figure 2.1 shows the Relativistic Heavy Ion Collider (RHIC) layout. In this section, we highlight the "Siberian Snake", beam indication, beam energy, beam polarization and collider luminosity. RHIC's accelerator complex enables the sustained polarized protons which is an only circular collider with this unique capability in the world. A special structure, called "Siberian Snake", prevents protons from depolarizing as they pass through the accelerator. "Siberian Snake" helps nearly 60 % of protons to be polarized. The two polarized beams circulate around the ring in opposite directions and are called the "yellow" and "blue" beams. For 2012 data, the center of mass energy was $\sqrt{s} = 510\,GeV$ which is $255\,GeV$ for each yellow or blue beam.

2.2   STAR Detector
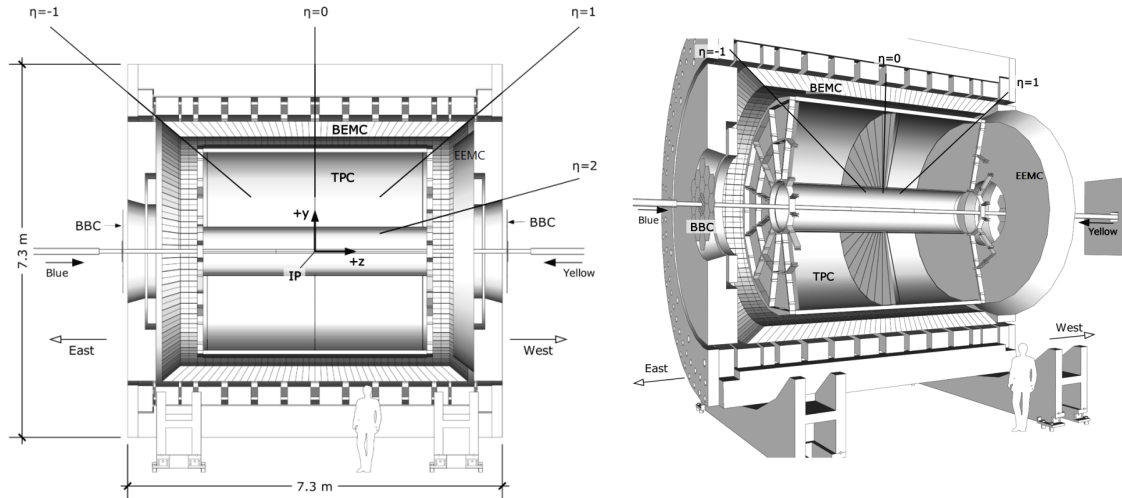
2.2.1   Detector Geometry

Figure 2.2: Schematic of the STAR detector

Figure 2.2 shows the STAR detector components. The STAR detector has full azimuthal coverage. Figure 2.2 shows two important structures of the STAR detector, the BEMC and EEMC. The Forward Meson Spectrometer (FMS), not labeled in Figure 2.2, is located near the beamline. Pseudo-rapidity (η) is a spatial coordinate describing the angle of a particle relative to the beam axis. For our analysis we analyze pi0s detected by the EEMC, which occupies a specific pseudo-rapidity region ($1.1 < \eta < 2.0$).

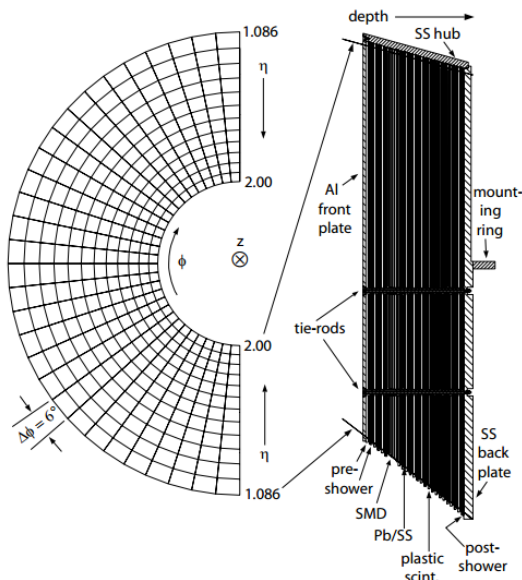## 2.2.2 The Endcap Electro-Magnetic Calorimeter (EEMC)

Figure 2.3: EEMC tower structure

Figure 2.3 is the EEMC tower structure. The left half-circular view shows the subdivision of EEMC into 720 towers. The longitudinal segmentation of the tower is presented on right side of the plot. Each tower consists of 23 layers of lead/stainless steel absorber and 24 layers of plastic scintillator. Each tower has pre-shower, post-shower, and shower maximum detector layers which are read out separately from the main scintillators. As photon or charged particle travels through the calorimeter, it leaves energy blobs at each layer. By adding the deposits, we can identify the photon energy. Among the tower layers, there is a two-layered segment called Shower Maximum Detector (SMD) that precisely locates the photon, electron or positron.

Shower-maximum detector (Figure 2.4) is a useful segment that can precisely measure the position of energy deposits from photons and help distinguish photon from electrons and other charged particles. Each U and V SMD plane contains extruded polystyrene-based scintillator strips and adjacent U and V sectors are placed in full azimuthal coverage. U-plane and V-plane have specific diagonal fiber arrangements in order to figure out the photon location.
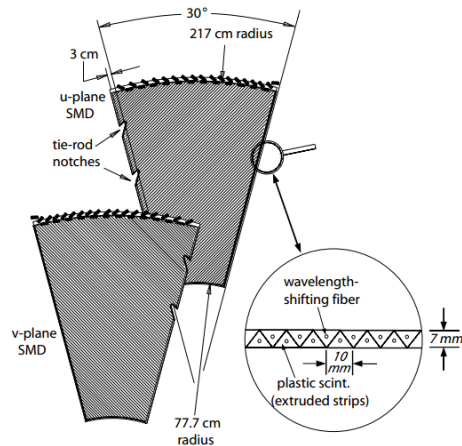
Figure 2.4: Shower-Maximum Detector (SMD)

2.2.3   EEMC Trigger

We used Endcap High Tower trigger (EHT0) for the analysis and trigger threshold energy equals to $E_T = 5.7\,GeV$. E_T is the transverse energy that the transverse represents direction perpendicular to the proton beam-line. The trigger records events if the transverse energy recorded in one tower is more than $5.7\ GeV$. Compared to other types of particles, photons tend to deposit most of their energy in a small number of towers, so this is a useful trigger geometry for identifying events with photons. This triggering process helps to select the potentially interesting events with reduced data file sizes since for many $p + p$ collisions, we only have limited capacity to record a certain number to disk for later analysis.

2.3   Analysis Process
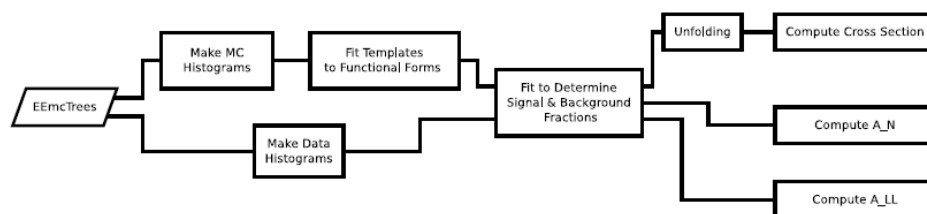
Figure 2.5: Analysis process of $\pi^0\,A_{LL}$ analysis

The analysis start from the raw data files called MuDST which contains all information about the collision events without any applied calibration. Based on MuDST files, we generate data accessible files called "Tree". Tree making constrains the STAR detector region

to be Endcap. Data Trees consists of Part 1, 2 and 3; Part 1 tree includes calibrated events, tower and SMD energies, and trigger information. The part 2 tree includes identified photon cluster at SMD strips and hit information. This part 2 tree does not have photons. It has clusters of SMD strips that have passed an algorithm that I will describe later. The part 3 tree contains photon and π^0 information, without any trigger cut yet having been applied, and without any separation into different spin states. At this point position information from the SMD strips has been combined with energy from the towers into photons, and then into π^0s. Using the part 3 photon data, π^0 gets reconstructed for all photon combinations since it is impossibly to know which photons, in a multi-photon event, come from a particular π^0 decay. Based on data trees, data histogram is produced with separated spin state as well as specific transverse momentum (p_T) cut. p_T represents the energy of the particle (higher p_T means that the particle has higher energy). Transverse momentum (p_T) is often used in collider physics, indicating the momentum of particle in a perpendicular direction to the longitudinal (beam-line) direction. In this process, we specify the events recorded by particular trigger, EHT0. Parallel to the data machinery, as shown in Figure 2.5, Monte Carlo (MC) simulated dataset follows the similar process up to tree making stage. This tree carries the particle ID so that we can extract the real π^0 from the mass distribution. Since the mass distribution was made from all photon combinations, there are wrong photon combinations that will be considered as one of the background factors. These MC trees are the basic ingredients to create template fits with adjustable fit parameters, which will be discussed in later section. The templates are separated in specific p_T range. By fitting and comparing templates to the data, we can determine the number of π^0 at specific spin state at p_T range. Identified π^0 counts are used for further A_{LL} calculation. For this research, I did not progress the unfolding and transverse asymmetry (A_N) calculation.

2.3.1   Software Used for the Analysis

The major software for the analysis is ROOT developed by Conseil Européen pour la Recherche Nucléaire (CERN) [8]. It is a modular scientific software framework to deal with big data processing, statistical analysis, visualization and storage. STAR collaboration uses ROOT version 5 with different release versions[1] are mainly written in C++. The existing analysis infrastructure in StRoot library at STAR collaboration website[2].

2.3.2   Photon Reconstruction Process

We begin reconstructing photons by building clusters of SMD strips. The Tukey-Smoother – IU (TSIU) SMD clustering algorithm is applied to each SMD sector and layer separately. This algorithm begins by applying the Tukey-Smoother for ten iterations, and then allowing all strips with energy above 2 MeV to serve as seed strips. This algorithm begins a hybrid clustering process proposed by former researcher, Steve Gliske [9]. The 3 strips on either side of the seed strip are assumed part of a cluster, total 7 strips will be identified as a set.

---

[1]All releases can be found at https://root.cern.ch/releases
[2]https://drupal.star.bnl.gov/STAR/comp/

The cluster must satisfy the following conditions:

1. The number of non-zero energy strips (before smoothing) is greater than 4

2. The total smoothed energy summed over all the strips is at least 3 MeV, and this is assigned to be the cluster energy

3. The energy after smoothing decreases monotonically from the seed strip. The cluster position is determined from the smoothed energy-weighted mean positions of the strips in the cluster.

After this process, identified clusters for each SMD layer are combined to make "points" with η and ϕ position. The tower records energy around the "point" and forms "hit" which is a combination of $\eta - \phi$ and energy. This hit is considered as a incident particle candidates and their momentum is computed based on the position and energy.

Chapter 3

π^0 Quality Assurance

3.1 Photon Clustering Differences

3.1.1 Change in ROOT Release Version

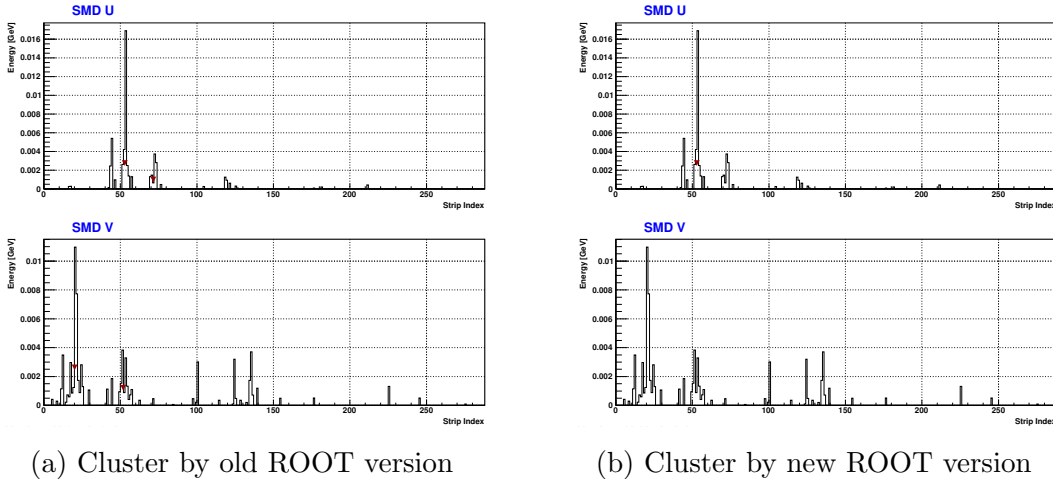(a) Cluster by old ROOT version   (b) Cluster by new ROOT version

Figure 3.1: Cluster differences depending on the ROOT version

The photon clustering process was changed due to ROOT version transition from 5.34.09 to 5.34.30. During the process of tree making, we cross-checked with our π^0 distribution peak to Yaping Wang who works on the similar analysis. We observed differences in generated π^0 distribution plot depending on STAR software version. After checking tree samples using different STAR libraries the major differences in π^0 counts originated from ROOT release version that plays major role in compiling codes. Histogram making code in ROOT version includes smoothing algorithm that converts raw data into analyzable peak with reduced statistical fluctuations. Internally, this algorithm should have included two iterations. One smoothing pass whose results are fed back into the algorithm for a second pass. Externally, we can then choose to call the algorithm multiple times. The result of each external iteration becomes the input for the next. In 2014 the ROOT developers realized that their implementation of the algorithm had only one internal iteration, and fixed the algorithm to include

both internal iterations. The 2006 STAR analysis, completed in early 2014, used the "old" ROOT version with one internal iteration. More recent STAR analysis inadvertently, based naively on "newer" versions of ROOT, inadvertently used two internal iterations.

More information can be found in https://sft.its.cern.ch/jira/browse/ROOT-6906

To study the issue, we can change the number of internal iterations by changing the version of ROOT that we use. We can change the number of external iterations in our own STAR code. Clustering differences is shown in Figure 3.1a and Figure 3.1b. From the 2006 data analysis note [9], internal iteration was set as 10 (by Steve Gliske). The major effect due to the ROOT debug is the number of cluster identified as a photon hit. Two exact same data signals on SMD strips passed through the smoothing process and verifies 2 clusters from each U and V strip. However, the new version of ROOT does not identify the clusters that satisfy the "requirements to be considered as a cluster." Therefore, the number of reconstructed photons and π^0s will be different (shown in following figures).
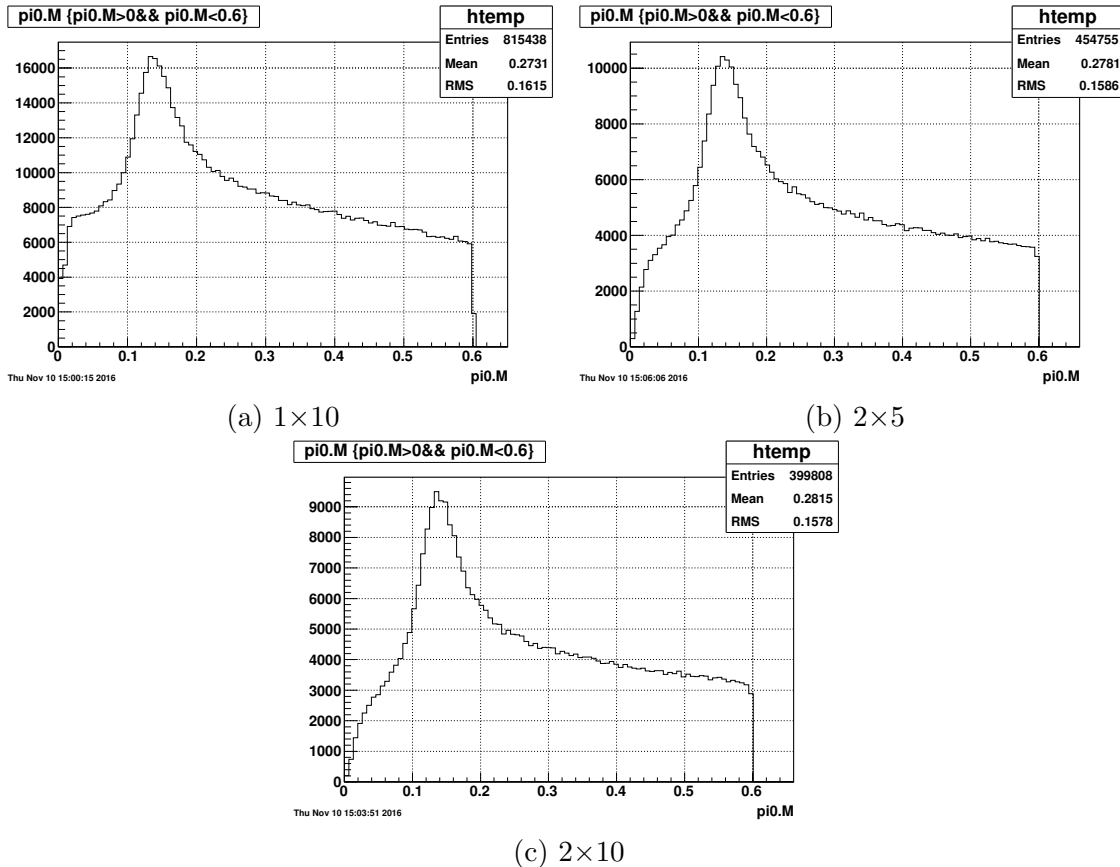

(a) 1×10

(b) 2×5

(c) 2×10

Figure 3.2: π^0 mass distribution differences due to smoothing

Figure 3.2 shows three different comparisons of π^0 mass spectrum. For this comparison, we did not apply any trigger cut, spin separation or p_T cut. Each figure caption denotes the number of smoothing done on raw data sample. 2×5 means that each number in figures

19

above represents [Number of calling SmoothArray by ROOT]×[Iteration in SmoothArray]. In figure captions of Figure 3.2, we'll use labels like 2×5. The "2" refers to the number of internal iterations, the "5" refers to the number of external iterations. As we will present the change in algorithm is not as simple as just a number of iterations, but this labeling provides one way of exploring the issue.

In Figure 3.2, there are significant difference in statistics due to the change of ROOT debug. Between Figure 3.2a and Figure 3.2c, one internal iteration of smoothing gives two times more entries. This difference originates from the previous clustering of the photon. As shown in Figure 3.1, ROOT version before bug-fix was able to identify up to four photons from SMD. However, new ROOT version does not have any identified clusters on SMD V. These number of photon differences causes significant deviations in π^0 mass distribution plot. In addition to this statistical aspect, the shape of left shoulder for Figure 3.2a becomes smoother after the debug, as shown in Figure 3.2c. As an intermediate cross-check, Figure 3.2b (2×5) was generated to check the difference from 1×10 case. With naive assumptions, the equal total iteration of smoothing was supposed to give similar results; however, 2×5 version is close to 2×10. The peak itself seems to be sharper for more iterations with lower background.
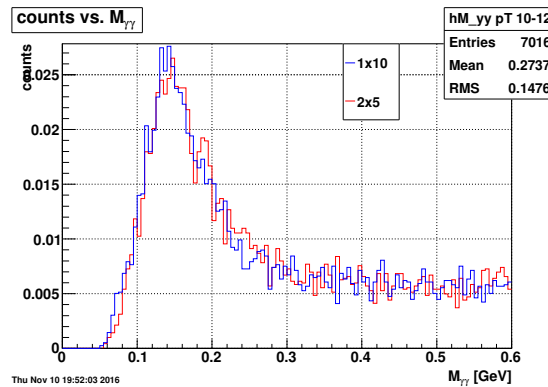
3.1.2 Clustering Iteration Comparison

Comparison of 1×10 **and** 2×5
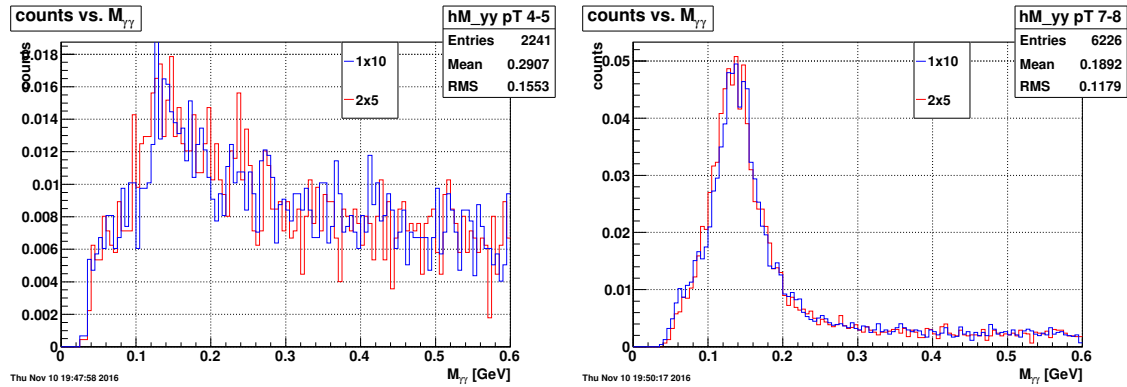
(a) $4GeV/c < p_T < 5GeV/c$

(b) $7GeV/c < p_T < 8GeV/c$

(c) $10GeV/c < p_T < 12GeV/c$

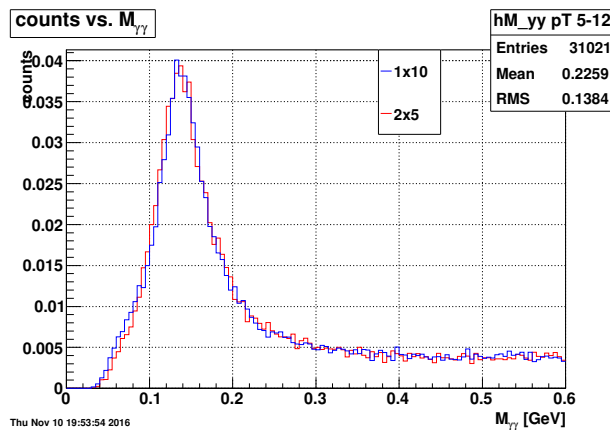Figure 3.3: Normalized π^0 mass plot at specific transverse momentum range (p_T)

Figure 3.4: Normalized mass spectrum $5GeV/c < p_T < 12GeV/c$

21

Figure 3.3 shows the shape of π^0 mass distribution depending on number of iterations in smoothing algorithm. We compared mass distribution at different p_T bins. After applying the EHT0 trigger, the total entries went down to 15 % differences in statistics. To check the shape between two mass distribution plots, we normalized the graph so that the area of distribution matches to 1. For Figure 3.3a, lower p_T bin has high statistical fluctuation. For higher p_T bins, there are no significant differences. Comparing this trigger applied distribution (Figure 3.4) and without any trigger selection (Figure 3.2), once we specify the EHT0 trigger, the difference in statistics decrease and we cannot clearly distinguish the discrepancies in shape of two distributions. We expect that the variations were filtered after applying the trigger cuts. Also, different from the background differences in Figure 3.2, once we require the trigger cut, therefore, significant background deviation gets eliminated.

Comparison of 1×10 and 2×10
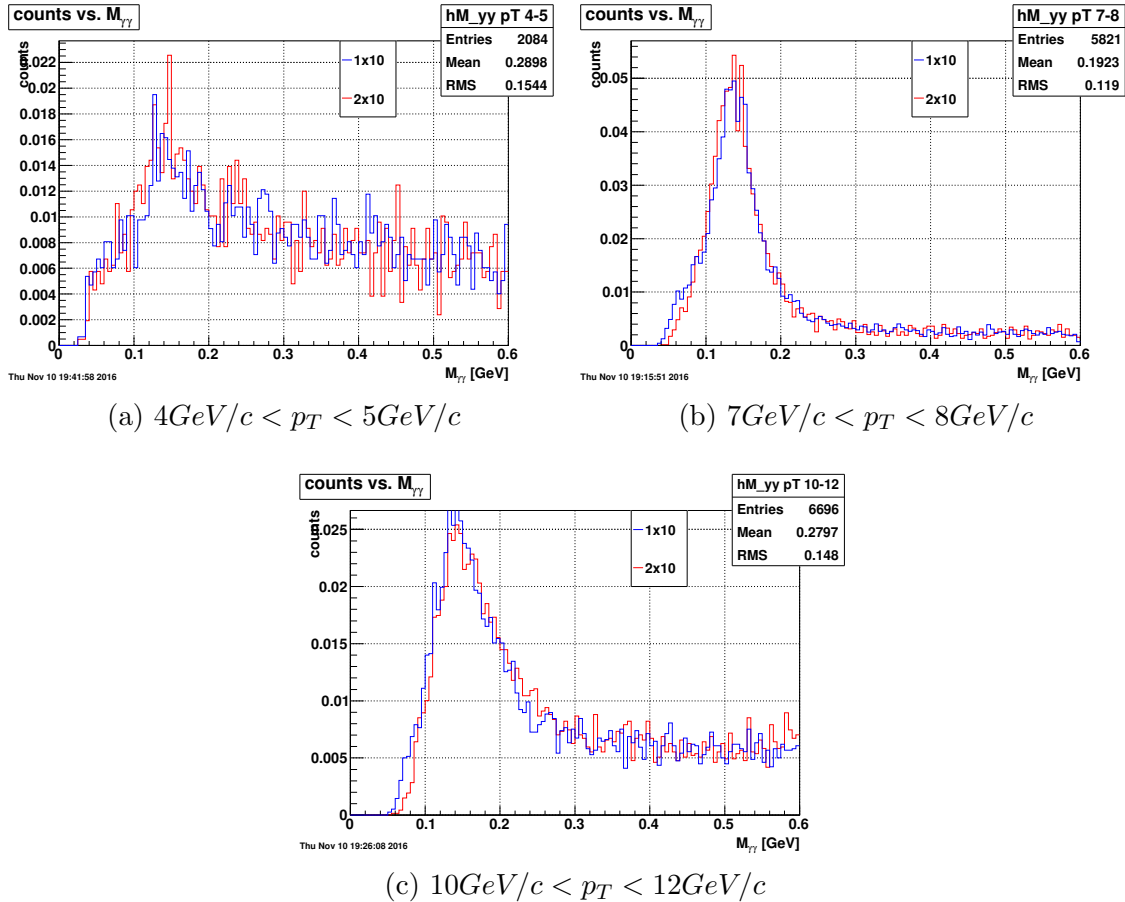

(a) $4GeV/c < p_T < 5GeV/c$

(b) $7GeV/c < p_T < 8GeV/c$

(c) $10GeV/c < p_T < 12GeV/c$

Figure 3.5: Normalized π^0 mass plot at specific transverse momentum range (p_T)
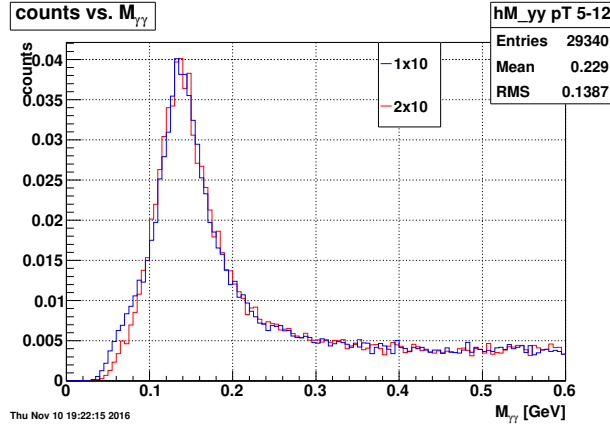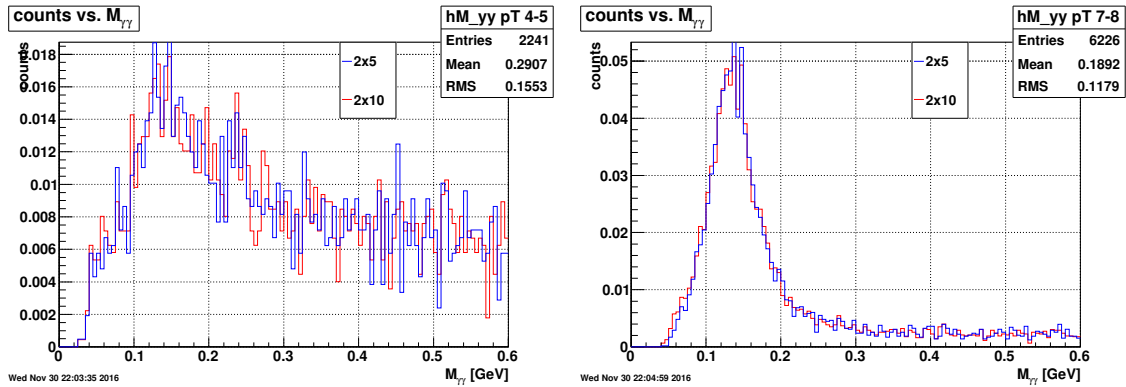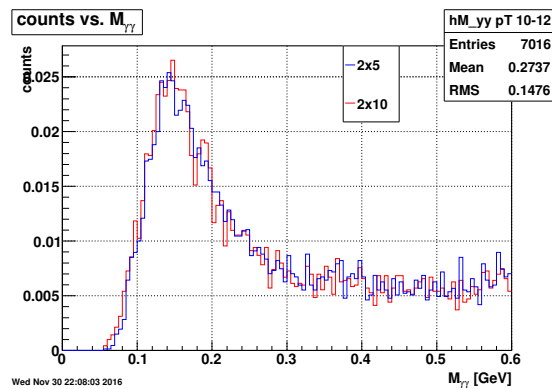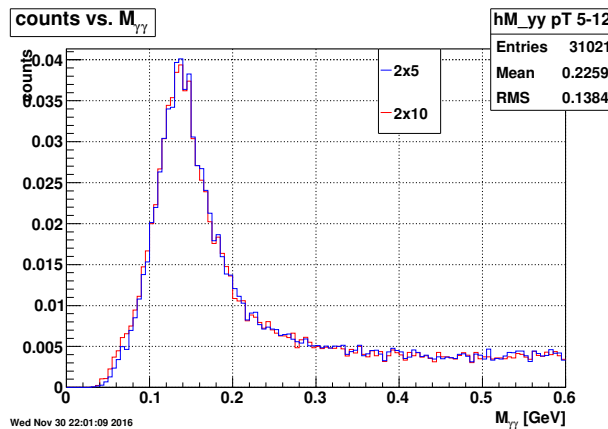
Figure 3.6: Normalized mass spectrum $5GeV/c < p_T < 12GeV/c$

In Figure 3.6, we compared the normalized peak results depending on internal clustering iteration. As mentioned in previous section, the left shoulder for one internal iteration shows discrepancy at intermediate and high p_T bins. In low p_T region (Figure 3.5a), it is hard to observe the clear differences due to low statistics. We conclude that the internal iteration affects the lower invariant mass section, yet we do not fully understand the correlation between internal and external iteration of this smoothing algorithm. From these two comparisons (Figure 3.4 and 3.5), we conclude that the internal and external iterations are more complicated than our assumption. Also the bug-fix of internal smoothing repetition does not significantly deform the mass distribution, but we do see some differences in lower mass part. We believe that the it is okay to use the bug-fixed ROOT version, which we expect to obtain clearer π^0 signal peaks for other triggers.

<div align="center">

Comparison of 1×10 and 2×10

</div>

As a consistency check, we also compared the mass distribution shape of 2×5 and 2×10. Figure 3.7 compares the normalized mass distribution plots depending on the external iteration. As shown in the figure, there are noticeable deviations from any of p_T range plots. For our p_T range of interest, both peaks overlap with small statistical fluctuation. Therefore, unlike to our hypothesis, the number of internal iteration affect the clustering identification more than the external iteration (a fine nob that users may change easily). Since the method of 2×5 is not different from other iteration methods, we conclude that 5 external iteration can be used for further data analysis.

(a) $4GeV/c < p_T < 5GeV/c$

(b) $7GeV/c < p_T < 8GeV/c$

(c) $10GeV/c < p_T < 12GeV/c$

Figure 3.7: Normalized π^0 mass plot at specific transverse momentum range (p_T)

Figure 3.8: Normalized mass spectrum $5GeV/c < p_T < 12GeV/c$

Chapter 4

Monte Carlo Simulation Studies

4.1   PYTHIA

PYTHIA is a computer simulation program for particle collisions at very high energies in particle accelerators. This simulates partonic collisions and produced particles that interact with the detector components. The simulated results are saved in a similar formation of unrefined data files. The files have structure named MuDST that can be refined into tree that goes through similar process as data tree. In addition to this, there is a Monte Carlo special tree that carries the particle identification. In general, the simulation results are segregated under ejected partonic p_T ranges. For 2011 Monte Carlo simulation, there are partonic bins of 2-3, 3-4, 4-5, 5-7, 7-9, 9-11, 11-15, 15-20, 20-25, 25-35, 35-45, 45-55, 55-65, 65-75, and 75-infinity (GeV/c) with different cross sections and number of collision events. Therefore, segregated partonic p_T bins have to be stitched together with weighting factor which is correlated to the cross section and collision numbers [10].

4.2   Fit Template

Template functions are fit from simulated collision events. Specifically, a signal template and two background templates are used. Monte Carlo simulated results are dealt as data analysis. Monte Carlo Tree contains reconstructed photon and π^0 events with specified particle identification which let us extract real pion mass peak since, for simulated events, we know specifically which photons come from which pi0 decays, and where photons interact in the detector. With the mass distribution peak, we apply fit in order to make template fit [See Appendix 7.3 for 2006 templates]. Signal fit is the actual π^0 signal where the reconstructed photons and π^0 match well to the real π^0s and photons, and conversion background indicates that the two reconstructed "photons" that formed the π^0 candidate but they are actually two pair-produced leptons from a photon that converted in material upstream of the EEMC [3]. The "other" background includes combinatorial background (from all photon pair invariant mass calculation), as well as backgrounds due to other reconstruction issues.

There was previous analysis of 2006 data had a simulated Monte Carlo events that were

applied to the data in order to extract the background. However, the energy of 2006 proton+proton collision events was 200 GeV, which is deviated from 2012 data, 510 GeV. We decided to use 2011 Monte Carlo simulation used for jet analysis ($p + p \rightarrow jet + X$). For the first step, we neglected the weighting factors [10] to check the mass distribution for individual reconstructed π^0 p_T range so that we can assure quality of the template.
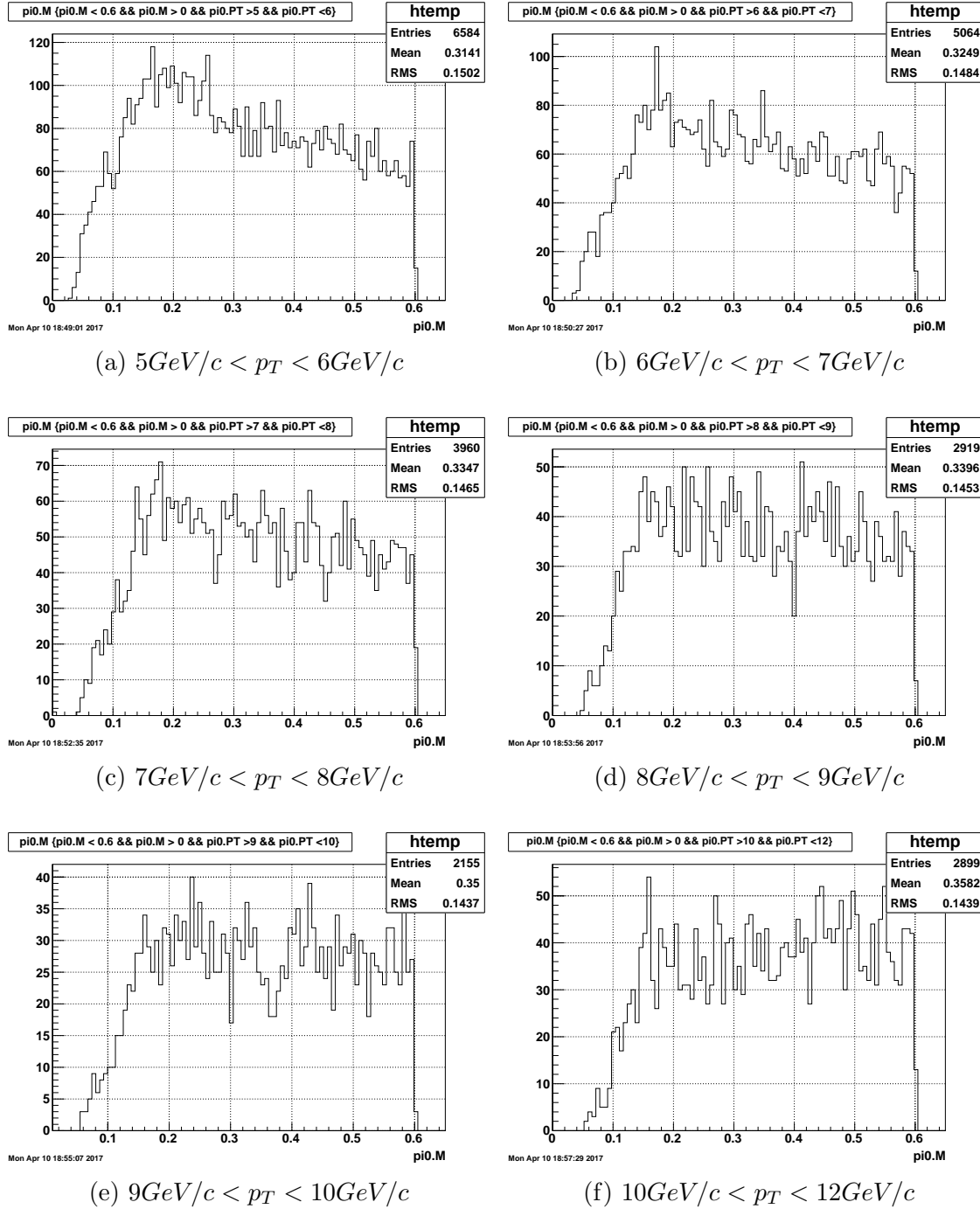

(a) $5GeV/c < p_T < 6GeV/c$

(b) $6GeV/c < p_T < 7GeV/c$

(c) $7GeV/c < p_T < 8GeV/c$

(d) $8GeV/c < p_T < 9GeV/c$

(e) $9GeV/c < p_T < 10GeV/c$

(f) $10GeV/c < p_T < 12GeV/c$

Figure 4.1: Reconstructed Monte Carlo data at specific transverse momentum range (p_T)

Figure 4.1 shows the collection on 2011 template without specific trigger selection. Therefore, we expect number of entries to be lower than what is shown in the figure and we do not insist that the 2011 Monte Carlo contains enough pion counts at EEMC region. In addition to the low entry issue, we are not able to observe the clear π^0 mass peak near 135 MeV/c^2 as shown in 3.2b. In addition to indistinguishable pion peak, each p_T bin contains low entries to create sufficient template. As a result, there are not sufficient events of π^0 so we are not able to construct the template that can be compared to the real 2012 data.

In order to observe the problem, we extracted the plot from specific p_T between 7 GeV/c and 8 GeV/c, in following figure 4.2b. This particular plot shows the identified pion mass distribution that can be used for the fit that can create the template fit of π^0 signal.
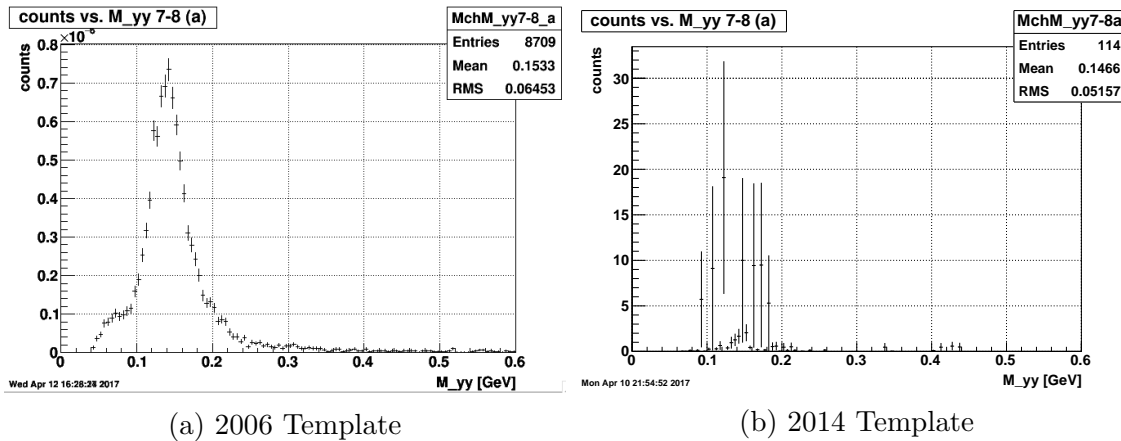

(a) 2006 Template   (b) 2014 Template

Figure 4.2: Comparison of template at $7 GeV/c < p_T < 8 GeV/c$

This plot is generated during process of making template. Template making applies the particle ID under the mass distribution so that we can segregate π^0 as shown in figure above. Also, the weighting factor is applied in order to stitch different partonic pT results.

According to the 2006 template figure 4.2a, there is an obvious π^0 mass peak with sufficient entries (8709 entries) to create the template fit. However, 2011 template figure 4.2b has neither obvious shape nor enough statistics (114 entries).

Due to the adequacy issue of 2011 simulated events, for following results, we will use 2006 templates to observe whether 2006 200 GeV template is reasonably applicable or not. As a substitution of template method, we make crude fit using simple Gaussian curve with exponential background curve (for the fitting, we used IGOR pro software). Based on fits, we performed sample calculation of A_{LL} for 2012 dataset.

Chapter 5

Results

5.1 Fitting Results

Dataset collected by RHIC has specific divided sets, specifically, accelerator gets filled with protons that moves along the path and these proton collections are called "fill". After 8 hours of proton collisions, the "fill" is removed from the accelerator and replaced with the new "fill". And this "fill" gets divided into 10-16 "runs" which is a recording for 2 million events. These sub-division processes let us enhance the data efficiency.

Currently, we have 497 "runs" saved on High Performance Storage System (HPSS) at RHIC. HPSS is software that manages large sizes of data on robotic tape libraries [2012 data trees are saved on /home/tkim1/Run12Tree/]. Due to the large number of runs, we decided to subdivide into multiple groups. We will provide results at individual run, one fill, and multiple fills with similar relative luminosity. This may lead us to the comparison from smaller dataset to larger data.

2006 templates shown in Figures, 7.1, 7.2 and 7.3, are used for 2006 data analysis. The template fitting code finds the best fit result that is a linear combination of three templates: signal, conversion background and other background. Reduced chi-square check is done to check the validity of the fit and the energy fraction (the location of peak ratio between data mass distribution and Monte-Carlo mass distribution). From the fit, we use both histogram and fit-function information to determine the number of π^0. Since the simulated collisions had center of mass energy of 200 GeV, results are not adequate or complete. Therefore, we decide to apply simple fit to figure out number of π^0.

5.1.1   Single Run Fit with 2006 Template

(a) $5 GeV/c < p_T < 6 GeV/c$

(b) $6 GeV/c < p_T < 7 GeV/c$

(c) $7 GeV/c < p_T < 8 GeV/c$

(d) $8 GeV/c < p_T < 9 GeV/c$

(e) $9 GeV/c < p_T < 10 GeV/c$
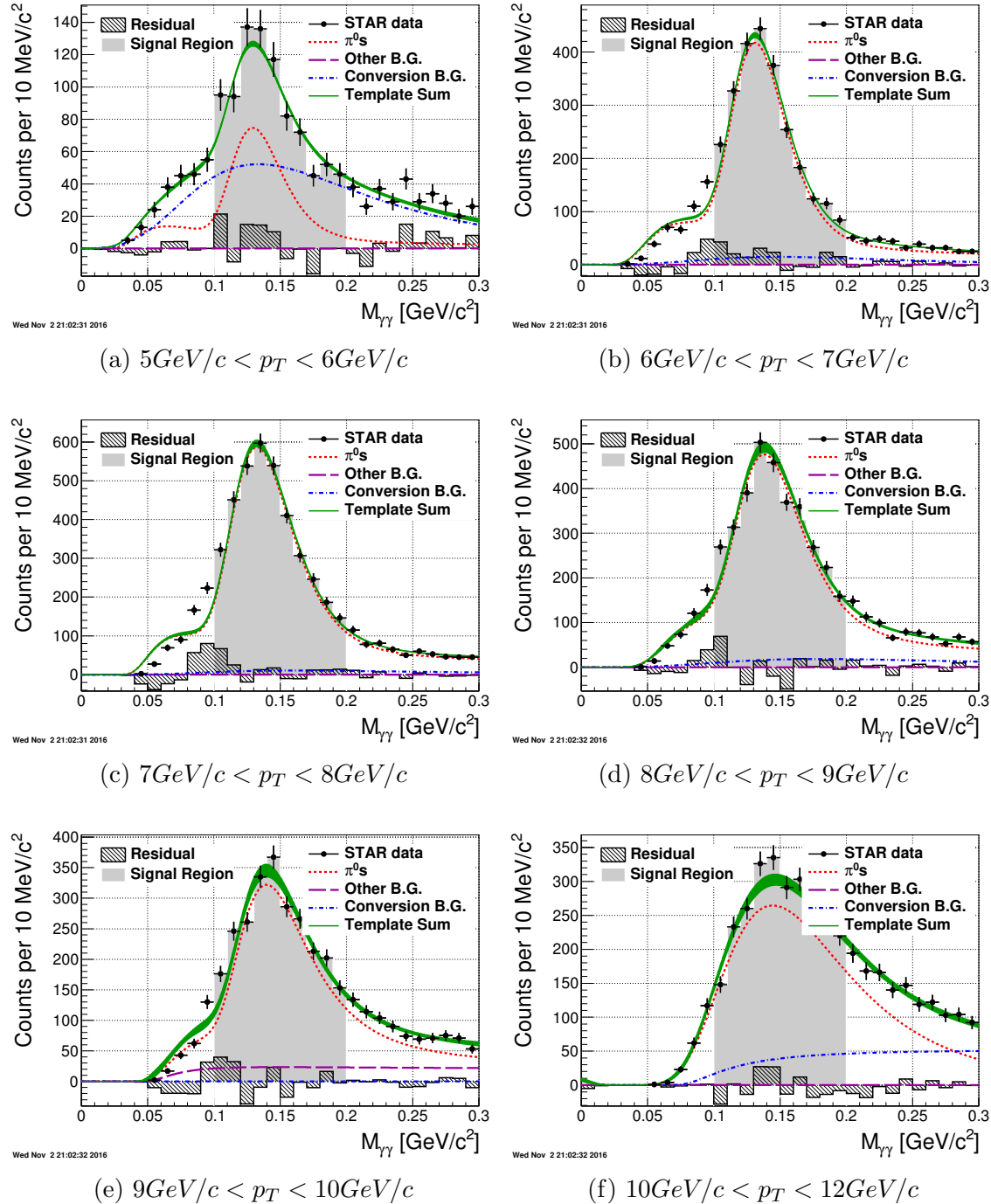
(f) $10 GeV/c < p_T < 12 GeV/c$

Figure 5.1: Mass plot fitting at specific transverse momentum range (p_T)

Figure 5.1 shows the fit results for a single run with run ID of 13081004. Each figure represents template fits at specific transverse momentum range. From this fitting process, the fitting was done under our interest region $(0 \, GeV/c^2 < M_{\gamma\gamma} < 0.3 \, GeV/c^2)$, yet, the number of π^0 was measured within the constrained mass range $(0.1 \, GeV/c^2 < M_{\gamma\gamma} < 0.2 \, GeV/c^2$, in Fig-

ure 5.1, the region is shown as gray area). In the fit plot, residual is shown to indicate the deviation between template sum fit (green line) and the data points (black dots). We are able to observe constant appearing of residual at left shoulder ($0.08\,GeV/c^2 < M_{\gamma\gamma} < 0.12\,GeV/c^2$), shown in figure 5.1b, 5.1c and 5.1d. This fitting was done without a separation of protons' spin orientation. For all p_T, we are not able to see any clear background contributions which lead us to conclude that either one run does not have enough statistics to identify clear separation of backgrounds, or 2006 template is not applicable due to the collision energy differences.

5.1.2   Multiple Runs Fit with 2006 Template

Our major for the fitting is not only see the π^0 signal under our interest region but also to identify clearer background contributions. Following figure shows the previous fitting results using 2006 data with 2006 template.
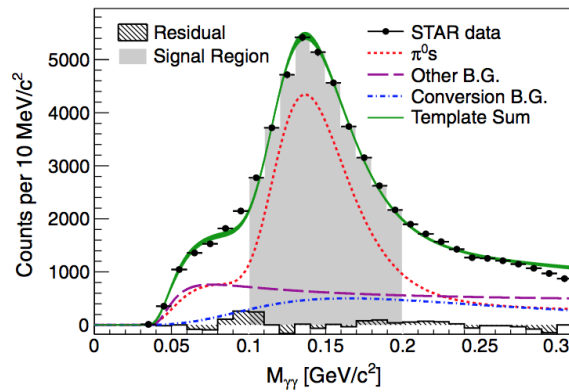
Figure 5.2: $7GeV/c < p_T < 8GeV/c$ fit result from 2006 data analysis [3]

For this section, we will investigate the validity of 2006 templates applied to large statistics 2012 data. We used 228 runs in order to compare with single run fit case, or investigate different helicity states of colliding protons.
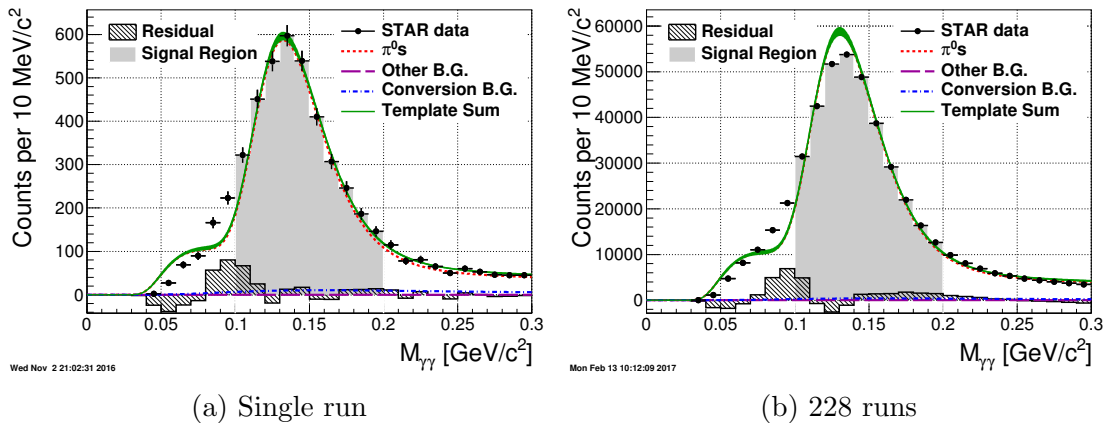
(a) Single run   (b) 228 runs

Figure 5.3: $7GeV/c < p_T < 8GeV/c$ Comparison

Figure 5.3 is the fitting comparison that may provide the evidence of differences between 2012 and 2006 data without any helicity separation. First, we focus on whether the claim that we made was valid. In the previous section, we questioned that either one run does not have enough statistics to identify clear separation of backgrounds, or 2006 template is not applicable due to the collision energy differences. As comparing single run and multiple runs, there are similar trends which are sharp left respect to the signal region and lower background at higher $M_{\gamma\gamma}$. These similarities are deviated from what we obtained from the 2006 data fitting results. The major difference between 2006 and 2012 is the statistical aspect. As shown in the figure 5.2 and 5.3b, peak point under the mass distribution for 2012 data is nearly 10 times bigger, and considering 228 runs are about 45 % of total 2012 runs, we expect to find more π^0s that lead us to reduce the statistical uncertainty. In addition, 2012 dataset has lower background than 2006 data. As shown in figure 5.2, right side of the signal region has larger background contribution (5200 counts maximum and 1000 counts background under π^0 mass distribution). For 2012 data, there are near 52000 counts at maximum point and about 5000 counts of background which has significantly less background fraction.
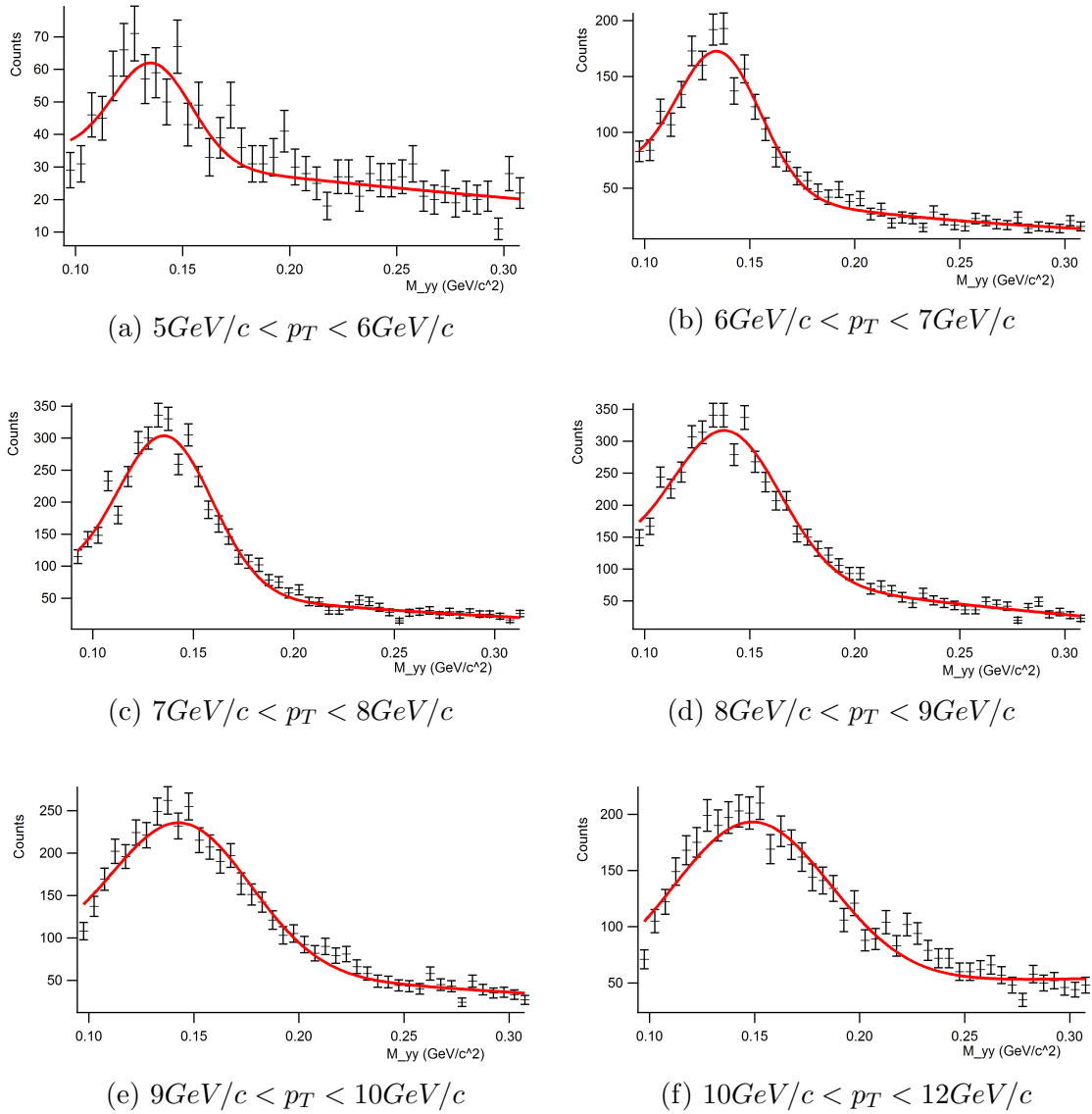
5.1.3   One Fill Analysis

(a) $5 GeV/c < p_T < 6 GeV/c$

(b) $6 GeV/c < p_T < 7 GeV/c$

(c) $7 GeV/c < p_T < 8 GeV/c$

(d) $8 GeV/c < p_T < 9 GeV/c$

(e) $9 GeV/c < p_T < 10 GeV/c$

(f) $10 GeV/c < p_T < 12 GeV/c$

Figure 5.4: One "Fill" mass plot fitting at specific helicity state (++)

Figure 5.4 shows naive fit results using program named IGOR[1] for one specific "fill". The "fill" ID was 16597 which includes run number 13081003, 13081004, 13081005, 13081006 and 13081007. The fit function was Gaussian π^0 signal with exponential background. The x-axis domain was set from 0.0975 GeV/c^2 to 0.3075 GeV/c^2. In addition to this $++$ spin state, same fitting was done for other spin states. Based on number of π^0 under the Gaussian distribution, we calculate A_{LL} for each p_T bin (the result A_{LL} is shown in later section).

---

[1]More information about IGOR pro can be found in http://www.wavemetrics.com/products/igorpro/igorpro.htm
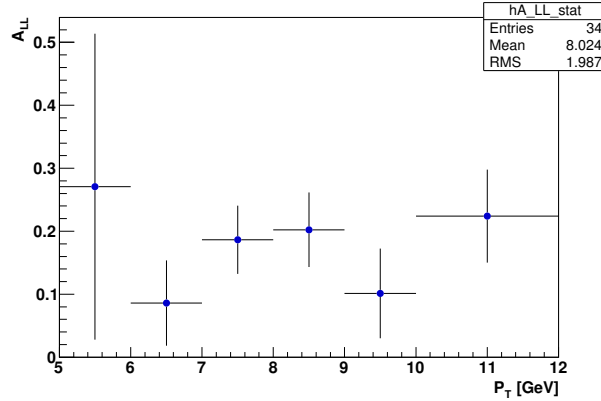
5.2 A_{LL} Results

Figure 5.5: Single run result of A_{LL}

Figure 5.5 shows A_{LL} result from the single run, 13081004. The π^0 signal is extracted using the 2006 Monte Carlo template. The result is calculated using equation 1.9 for specific p_T range. As explained in 2006 and 2012 data mass distribution, 2012 data has less background than 2006 data. Therefore, we expect 2006 Monte Carlo cannot be properly applied to the 2012 data. Also, A_{LL} results are not confident since we still use 200 GeV Monte Carlo simulated template with wrong smoothing version. The asymmetry values are significantly higher than previously published paper [3], as well as lower statistics, a single run out of total 497 runs in 2012 data.

p_T bin	++ helicity		+− helicity		−+ helicity		−− helicity	
	π^0 counts	error	π^0 counts	error	π^0 counts	error	π^0 counts	error
$5-6\ GeV/c$	278.99	16.70	226.22	15.04	386.25	19.65	298.11	17.27
$6-7\ GeV/c$	1239.71	35.21	1328.14	36.44	1291.46	35.94	1228.33	35.05
$7-8\ GeV/c$	2839.65	53.29	2437.48	49.37	2407.37	49.06	2998.32	54.76
$8-9\ GeV/c$	2875.64	53.62	2495.58	49.96	2633.61	51.32	3357.78	57.95
$9-10\ GeV/c$	2819.08	53.09	2204.92	46.96	2812.07	53.03	2833.25	53.23
$10-12\ GeV/c$	2684.92	51.82	2071.55	45.51	1871.28	43.26	2284.32	47.79

Table 5.1: 2012 single fill result
Each 'π^0 counts' column is identified from figure 5.4. Specifically, we integrate Gaussian peak, based on figure 5.4 fitting results, over all $M_{\gamma\gamma}$ in order to extract the number of π^0 and the error values are calculated based on Poisson statistics. $\sigma = \sqrt{\pi^0\ Counts}$

Table 5.1 is the result from the naive fit results shown in figure 5.4. We used equation 1.9 with relative luminosity value of $R = 1.075097$, polarization of blue beam of $P_B = 0.529721$ and polarization of yellow beam of $P_Y = 0.583791$. The error of individual constants are not accounted for calculating A_{LL} error using error propagation formula. Even though error contributions of relative luminosity (R) and polarization (P), we will modify the final A_{LL}

33

error formula. Following figure 5.6 is the A_{LL} for one fill. Comparing this to the one run A_{LL} (figure 5.5), we observe similar shapes after $p_T = 7\ GeV/c$. However, A_{LL} before the p_T is significantly different.
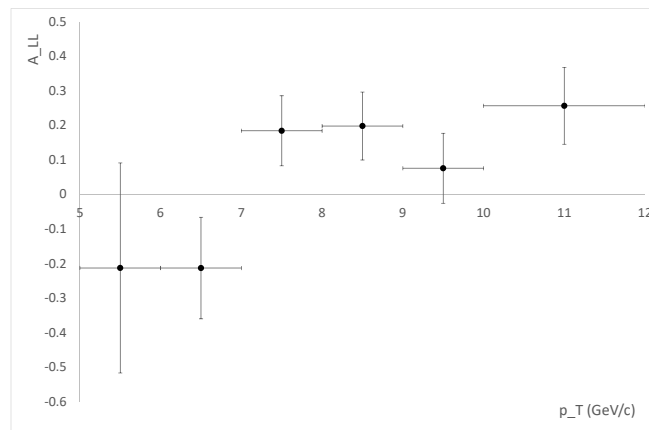

Figure 5.6: Single fill result of A_{LL}

Also, we still are under debate, yet not our priority, over the way of segregating data runs. As shown in two cases study of single run and single fill, overall statistical uncertainty is still relatively high due to the low number of π^0. These results are the preliminary sample check in order to verify whether the transition of adapting dataset from 2006 to 2012 works without problems, and single fill analysis in order to probe naive statistical check. The templates are not valid due to the energy difference, the simulated detector differences and significantly the shape of data mass distribution. Frankly, 2012 mass distribution creates low background with clearer π^0 peak; however, fill-by-fill analysis will not be a sufficient dataset that can reduce the statistical uncertainty [9] [11].

Chapter 6

Current Status and Future Work

6.1 Work Done

My work started from learning the basic theoretical background of the STAR experiment. During this process, I was able to expose myself to learn the flow of the analysis, and how codes are tied together. The basic code infrastructure was constructed for 2006 data analysis; however, the code does not work for 2012 analysis due to STAR software updates and changes. This needs higher trigger energy cut as well as changing in trigger to high tower trigger (EHT0). Thus, we changed the codes so that they can be applied to the 2012 data. During this tree making process, we recognized the ROOT version updates that causes significant deduction of identified number of π^0. We compared the iteration dependency and the clustering, with using newer ROOT version. In addition, we debugged and evolved codes such as data accessible tree making code, tree based histogram maker, Monte Carlo template fit maker, data fitter, and A_{LL} calculation code. Specifically, in asymmetry calculation, 2006 analysis codes had implemented A_{LL} calculation of following equation [9],

$$A_{LL} = \frac{1}{P_Y \cdot P_B} \left(\frac{N_{++} - N_{+-} - N_{-+} + N_{--}}{N_{++} + N_{+-} + N_{-+} + N_{--}} - \frac{L_{++} - L_{+-} - L_{-+} + L_{--}}{L_{++} + L_{+-} + L_{-+} + L_{--}} \right) \qquad (6.1)$$

Equation 6.1 is based on approximation derived from equation 1.8, which we do not fully understand the intermediate derivation. However, for other STAR collaborators, equation 6.1 was commonly used, so we developed new A_{LL} calculating codes to cross-check for consistency. The results were close to each other and we decided to use STAR version temporarily (equation 6.1) since the values of relative luminosity are accessible. We obtained relative luminosity and polarization values from one of the collaborators, Zilong Chang. As shown in previous sections, we analyzed one run (out of 497 runs in 2012 data) for a sample calculation. These code updates for 2012 data were done for most of data analysis process yet there are several bugs in codes for Monte Carlo template maker. The tree making codes for Monte Carlo were debugged with small unidentified problems, and we are working on this. The process has been updated and presented to the VU-ANL STAR collaboration group. Also, the analysis was presented at the Division of Nuclear Physics (DNP) conference.

After the basic software bugfix, 2012 data tree making process of 497 runs was done and trees are stored on HPSS. However, we focused on the software consolidation before making trees as well as fixing Monte Carlo (MC) tree making process so that the code can be applied to the 2011 Monte Carlo simulation. Then, from the MC tree, we made a sample template in order to check the validity of 2011 MC simulation on 2012 data. We applied how to stitch generated MC trees using weights for separately simulated partonic p_T collision events. As a conclusion of current MC simulation, we believe that there is not a sufficient collision events that can provide enough π^0 under mass distribution peak that can be used to generate template fit for signal and backgrounds.

6.2   Future Work

In the process of the analysis, we use relative luminosity values from other collaborator without firm grasp, however, we will confirm the method of getting relative luminosity numbers from different sources with different values[1]. Once we have converged idea of process data analysis, we will proceed the analysis explained in 2.3 (after tree making). We have to decide the data segregation since each fill contains different number of collision events that will give distinguishable relative luminosity. There are options to apply fitting per run, per fill, or the whole dataset. For 2006 dataset, whole dataset was used with knowledge of raw luminosity. "Good runs" lists will be evaluated with clear collision events and be determined whether we use one whole 2012 data, per specific timeline, fill[2] or run-by-run. In an aspect of Monte Carlo simulation, we will investigate more about the 2011 sample. If we conclude that 2011 is not adequate for our 2012 data, this will be replaced by our own MC simulation.

---

[1]There are three contemporary relative luminosity values addressed by STAR collaborators: Zilong Chang, Christopher Dilks, and https://www.star.bnl.gov/protected/common/triggerPages.html

[2]Bucket or proton bunch that fills RHIC

Chapter 7

Appendix

7.1 Derivation of the Relative Luminosity

$$A_{LL} = \frac{1}{P_Y\,P_B} \cdot \frac{\frac{N_{++}}{L_{++}} - \frac{N_{+-}}{L_{+-}} - \frac{N_{-+}}{L_{-+}} + \frac{N_{--}}{L_{--}}}{\frac{N_{++}}{L_{++}} + \frac{N_{+-}}{L_{+-}} + \frac{N_{-+}}{L_{-+}} + \frac{N_{--}}{L_{--}}} \tag{7.1}$$

From Equation 7.1, each cross section terms can be re-written by factoring out symmetric and anti-symmetric collisions respectively under assumption that each symmetric and anti-symmetric collision has equal/similar luminosities ($L_{++} \simeq L_{--}$ and $L_{+-} \simeq L_{-+}$). Given these conditions, the produced π^0s will be similar/equal for symmetric or anti-symmetric collisions ($N_{++} \simeq N_{--}$ and $N_{+-} \simeq N_{-+}$). Therefore, following equation satisfies,

$$\frac{N_{++}}{L_{++}} + \frac{N_{--}}{L_{--}} \simeq \frac{N_{++} + N_{--}}{L_{++} + L_{--}} \tag{7.2}$$

Then, it provides following equation,

$$A_{LL} = \frac{1}{P_Y\,P_B} \cdot \frac{N_{++} + N_{--} - \frac{L_{++}+L_{--}}{L_{+-}+L_{-+}}(N_{+-} + N_{-+})}{N_{++} + N_{--} + \frac{L_{++}+L_{--}}{L_{+-}+L_{-+}}(N_{+-} + N_{-+})} \tag{7.3}$$

Equation 7.3, often written as [11]

$$A_{LL} = \frac{1}{P_Y\,P_B} \cdot \frac{N_{++} + N_{--} - R_3\,(N_{+-} + N_{-+})}{N_{++} + N_{--} + R_3\,(N_{+-} + N_{-+})} \tag{7.4}$$

where

$$R_3 = \frac{L_{++} + L_{--}}{L_{+-} + L_{-+}} \tag{7.5}$$

7.2   Run 12 Beam Information

7.2.1   Polarization Information

[CNI Polarimetry Group[1]]

STAR group tracks the polarization of colliding protons at each "fill" and the values are saved individually run by run in

/star/u/ tkim1/ offline/ paper/ psn0583/ 2006EEMCpi0paper/ CrossSectionLongAsym/ lumipol_backup/ Pol

7.2.2   Relative Luminosity

We use relative luminosity values provided by one of STAR collaborators, Zilong Chang, and they are saved individually run by run in

/star/u/ tkim1/ offline/ paper/ psn0583/ 2006EEMCpi0paper/ CrossSectionLongAsym/ lumipol_backup/ Lumi

7.3   2006 Monte Carlo Template

Following templates are used for 2006 data analysis with 200 GeV simulated collisions. Figure 4.1, 4.2 and 4.3 show the normalized template fits that will be applied to the data in order to determine the number of π^0. Each template is divided depending on p_T bins and the template fitting code performs linear combination of template fits at specific p_T bin. The templates are used to compare with the data plot, for example, the location of π^0 mass peak to set signal fraction and the number of π^0s.

---

[1]https://wiki.bnl.gov/rhicspin/Run_12_polarization
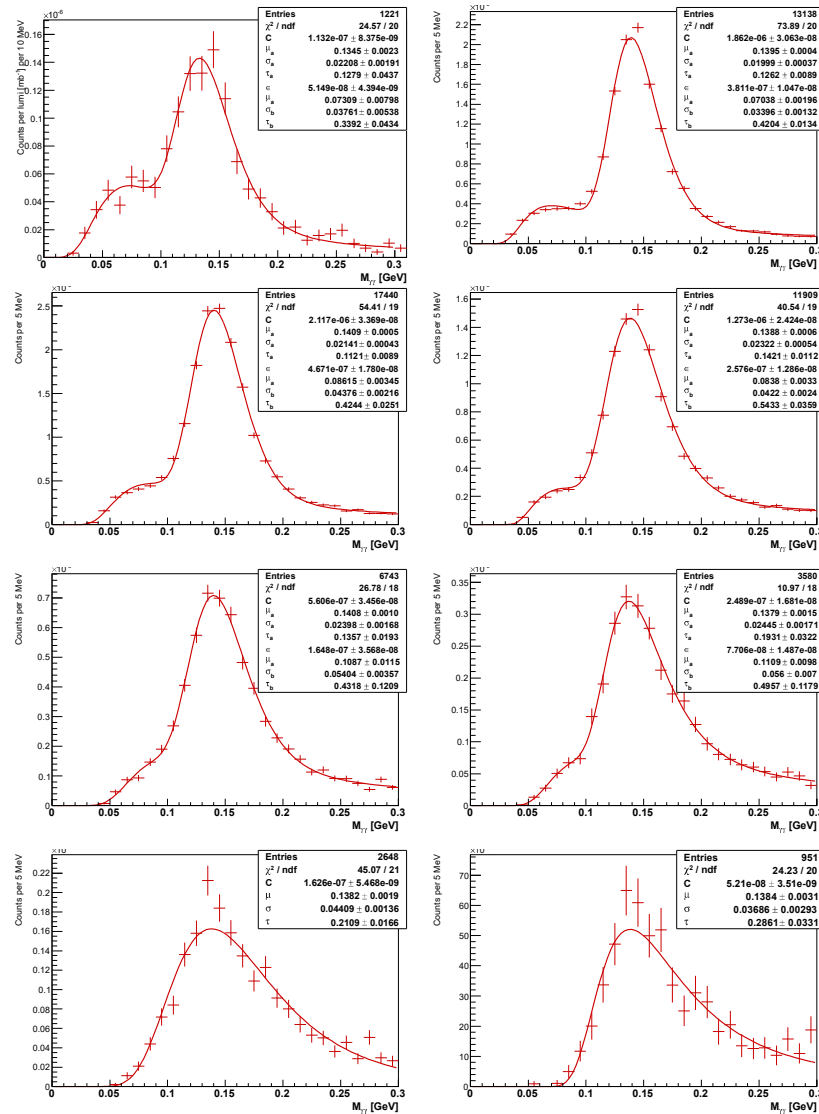
Figure 3.5: Signal shape fits: plot of the Monte Carlo data (data points with error bars) superimposed with the result for the template shapes (colored line). Plots are shown for each p_T bin, with the upper left being 4-5 GeV/c, upper right 5-6 GeV/c, second row left 6-7 GeV/c, and so forth.

27

Figure 7.1: Signal Fit
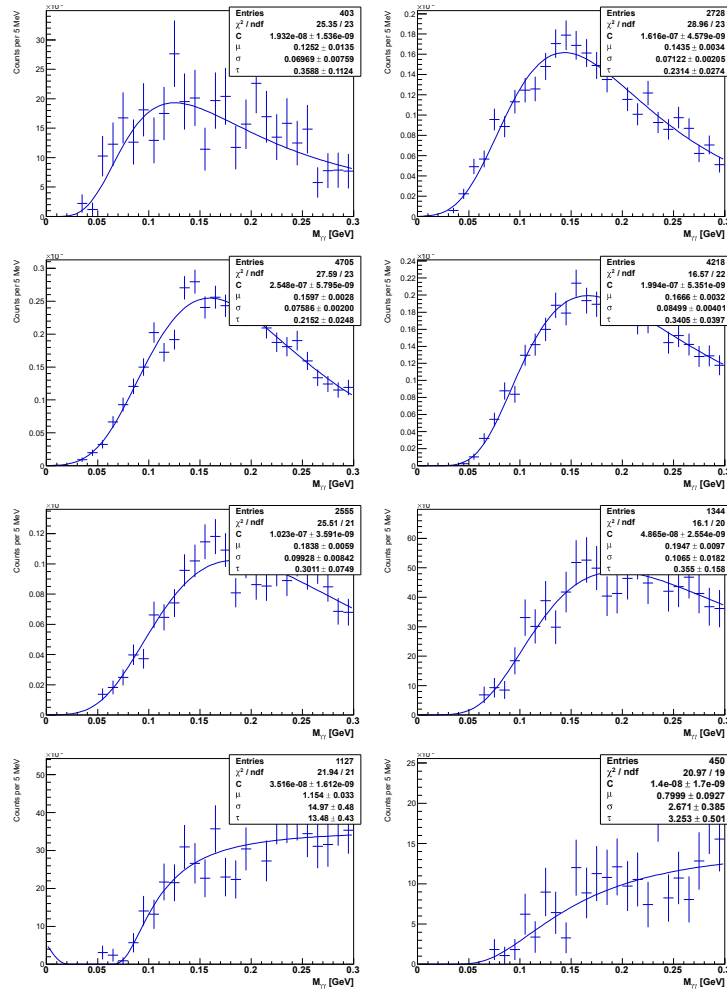
Figure 3.6: Conversion background shape fits: plot of the Monte Carlo data (black histogram) superimposed with the result for the template shapes (colored line). Panels are arranged as in Figure 3.5.

28

Figure 7.2: Conversion Background
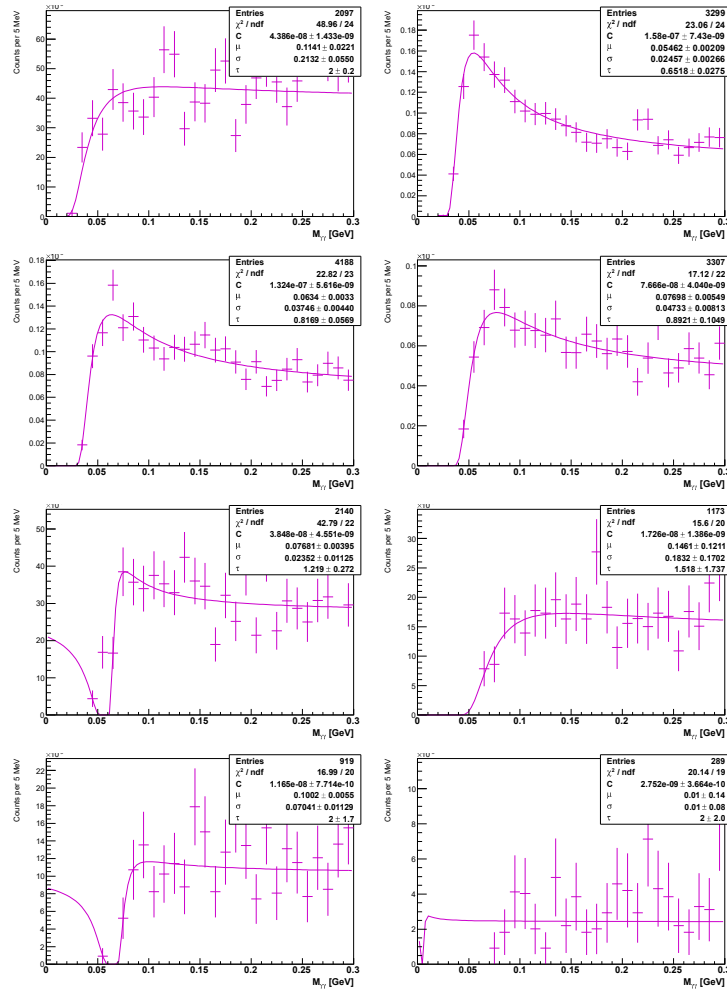
Figure 3.7: Other background shape fits: plot of the Monte Carlo data (black histogram) superimposed with the result for the template shapes (colored line). Panels are arranged as in Figure 3.5.

29

Figure 7.3: Other Background

41

7.4   2012 One Fill Fitting

7.4.1   Helicity $+-$
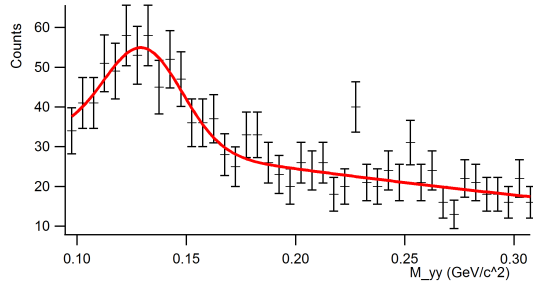
(a) $5GeV/c < p_T < 6GeV/c$
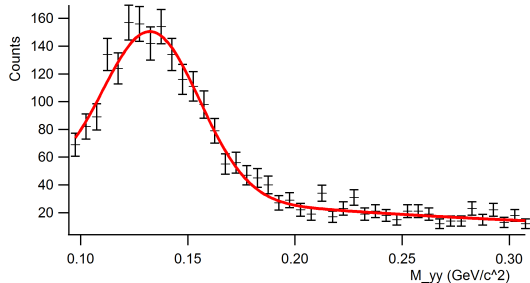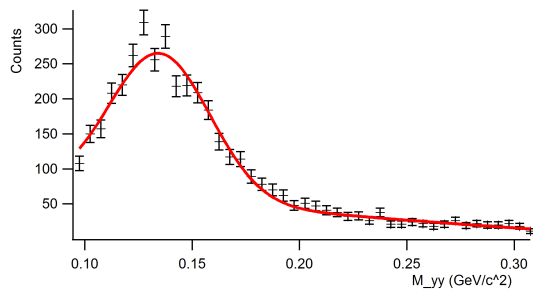
(b) $6GeV/c < p_T < 7GeV/c$
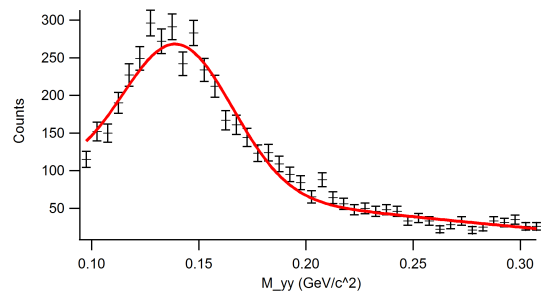
(c) $7GeV/c < p_T < 8GeV/c$
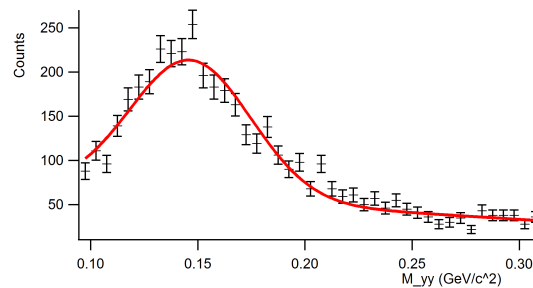
(d) $8GeV/c < p_T < 9GeV/c$
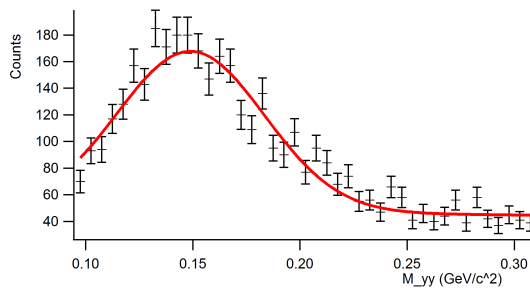
(e) $9GeV/c < p_T < 10GeV/c$

(f) $10GeV/c < p_T < 12GeV/c$

Figure 7.4: One "Fill" mass plot fitting at specific helicity state $(+-)$

7.4.2   Helicity −+
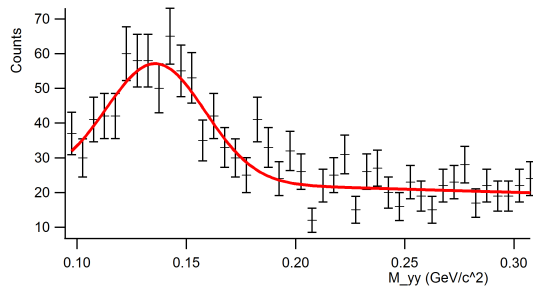
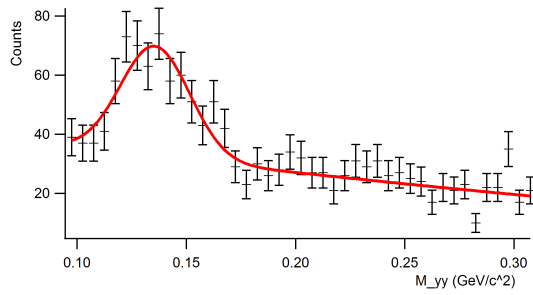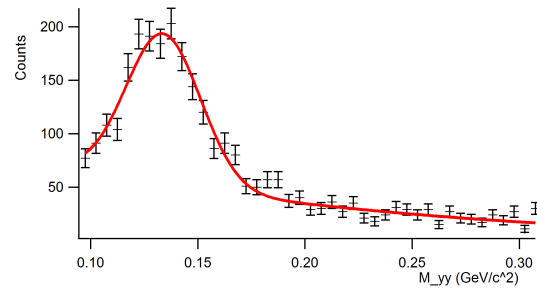(a) $5GeV/c < p_T < 6GeV/c$
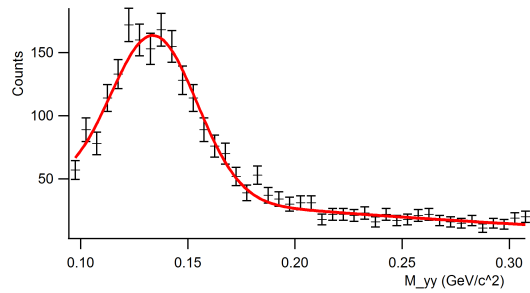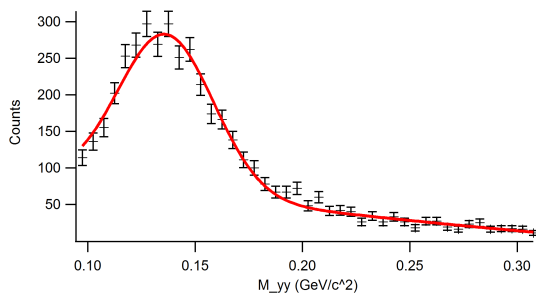
(b) $6GeV/c < p_T < 7GeV/c$
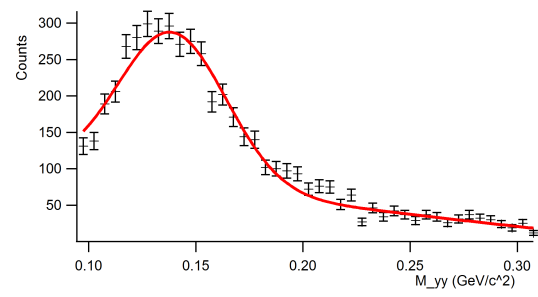
(c) $7GeV/c < p_T < 8GeV/c$
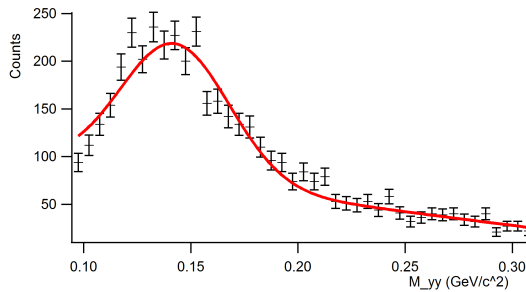
(d) $8GeV/c < p_T < 9GeV/c$
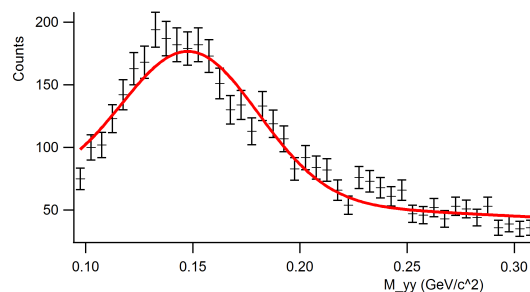
(e) $9GeV/c < p_T < 10GeV/c$

(f) $10GeV/c < p_T < 12GeV/c$

Figure 7.5: One "Fill" mass plot fitting at specific helicity state $(-+)$

7.4.3   Helicity −−

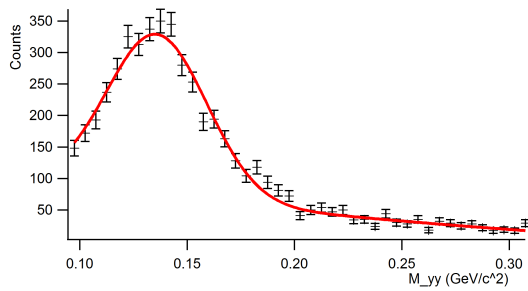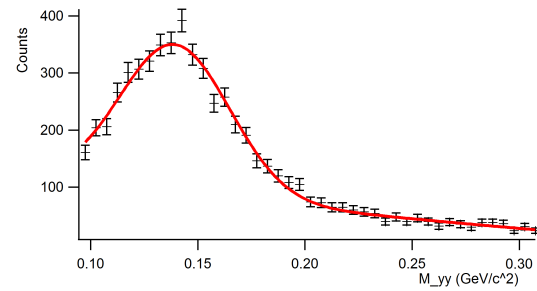(a) $5GeV/c < p_T < 6GeV/c$

(b) $6GeV/c < p_T < 7GeV/c$

(c) $7GeV/c < p_T < 8GeV/c$

(d) $8GeV/c < p_T < 9GeV/c$
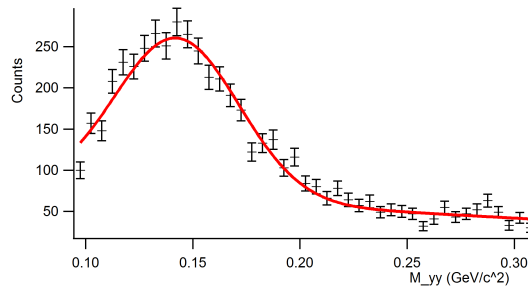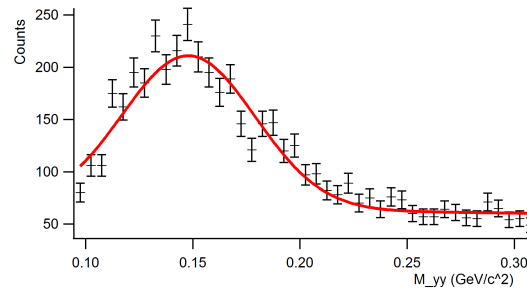
(e) $9GeV/c < p_T < 10GeV/c$

(f) $10GeV/c < p_T < 12GeV/c$

Figure 7.6: One "Fill" mass plot fitting at specific helicity state (−−)

Reference

[1] Florian D, Sassot R, Stratmann M, Vogelsang W. 2014. *Evidence for Polarization of Gluons in the Proton.* Phys. Rev. Lett.113.012001

[2] de Florian D, Sassot R, Stratmann M, Vogelsang W. 2008 *Global Analysis of Helicity Parton Densities and their Uncertainties.* Phys. Rev. Lett. 101, 072001.

[3] Adamczyk L et al (STAR Collaboration). 2014. *Neutral pion cross section and spin asymmetries at intermediate pseudorapidity in polarized proton collisions at $\sqrt{s} = 200GeV$.* Phys. Rev. D 89, 012001.

[4] Adare A et al (PHENIX Collaboration). 2007. *Inclusive cross section and double helicity asymmetry for π^0 Production in p+p collisions at $\sqrt{s} = 200GeV$: Implications for the polarized gluon distribution in the proton.* Phys. Rev. D 76, 051106(R)

[5] Aidala CA, Bass SD, Hasch D, Mallot GK. 2013. *The Spin Structure of the Nucleon.* Rev. Mod. Phys. 85, 655.

[6] Glück M, Reya E, Stratmann M, Vogelsang W. 2001. *Models for the polarized parton distributions of the nucleon.* Phys. Rev. D 63, 094005.

[7] He, Weihong. PhD, Indiana University. 2008. *Double Spin Asymmetry in Inclusive π^0 Production for Longitudinally Polarized proton proton collisions at $\sqrt{s} = 200GeV$ at the Endcap ElectroMagnetic Calorimeter at STAR.*

[8] Rene Brun and Fons Rademakers. *ROOT - An Object Oriented Data Analysis Framework.* Proceedings AIHENP'96 Workshop, Lausanne, Sep. 1996, Nucl. Inst. & Meth. in Phys. Res. A 389 (1997) 81-86. See also http://root.cern.ch/.

[9] Bridgeman A, Gliske S, Krueger K, Spinka H, Underwood D, Clark A, Drachenberg J, Gibson-Even A, Grosnick D, Koetke D et al. 2013. *Analysis Note for Run 6 EEMC π^0 Paper I & II.*

[10] Drachenberg J, Adkins K, Fatemi R. 2015. *Azimuthal Transverse Single-spin Asymmetries of Inclusive Jets and Charged Pions Within Jets from Polarized-proton Collisions at $\sqrt{s} = 500GeV$.*

[11] Hays-Wehle J, Seele J, Spinka H, Surrow B. 2011. *Relative Luminosity Analysis for run9 pp 200 GeV Running.*

Additional Works Consulted :

[12] Aschenauer EC et al. 2015. *The RHIC SPIN Program: Achievements and Future Opportunities.* arXiv:1501.01220.

[13] Grosse Perdekamp M, Yuan F. 2015. *Transverse Spin Structure of the Nucleon.* Annu. Rev. Nucl. Part. Sci. 65.1: 429-56.

[14] Leader, Elliot. 2005. *Spin in Particle Physics.* Cambridge: Cambridge University Press.

[15] Nocera E et al. 2014. *A first unbiased global determination of polarized PDFs and their uncertainties.* Volume 887, October 2014, Pages 276308

[16] Olive KA et al. 2015. *The Review of Particle Physics.* Chin. Phys. C, 38, 090001 (2014).

[17] Paetz, gen S. H. 2012. *Nuclear Physics with Polarized Particles.* Heidelberg: Springer.

[18] Rojo J, Ball RD, Debbio LD et al. 2009. *Update on Neural Network Parton Distributions: NNPDF1.1.* PUBDB-2016-01663

[19] Sakuma T, Walker M. 2011. *Dijet Cross Section and Longitudinal Double Spin Asymmetry Measurements in Polarized Proton-proton Collisions at $\sqrt{s} = 200 GeV$ at STAR.* J. Phys.: Conf. Ser. Journal of Physics: Conference Series 295: 012068.

[20] Abelev, et al (STAR Collaboration). 2009. *Longitudinal Double-Spin Asymmetry and Cross Section for Inclusive Neutral Pion Production at Midrapidity in Polarized Proton Collisions at $\sqrt{s} = 200 GeV$.* Phys.Rev.D80:111108,2009

[21] Aschenauer EC et al. 2016. *The RHIC Cold QCD Plan for 2017 to 2023: A Portal to the EIC.* arXiv:1602.03922v1

[22] Collins JC. Zu X. 2002. *Parton Distribution Functions Suitable for Monte-Carlo Event Generators.* J. High Energy Phys. 2002.06: 018.

[23] Collins JC. 2013. *Foundations of Perturbative QCD.* Cambridge: Cambridge University Press.